Localization of KANK2 to Focal or Fibrillar Adhesions Influences Migration in Melanoma Cell Lines

Nikolina Stojanović[1,*,#], Anja Rac[1,*], Marija Lončarić[1], Ana Tadijan[1,2], Mladen Paradžik[1,3], Marta Acman[1], Jonathan D. Humphries[4], Martin J. Humphries[5], Andreja Ambriović-Ristov[1,#]

[1]Laboratory for Cell Biology and Signalling, Division of Molecular Biology, Ruđer Bošković Institute, Zagreb, Croatia; [2]present address: Laboratory for Cell Biology, Division of Molecular Biology, Ruđer Bošković Institute, Zagreb, Croatia; [3]present address: Laboratory of Experimental Therapy, Division of Molecular Medicine, Ruđer Bošković Institute, Zagreb, Croatia, [4]Department of Life Science, Manchester Metropolitan University, Manchester, United Kingdom; [5]Manchester Cell-Matrix Centre, Faculty of Biology, Medicine & Health, University of Manchester, Manchester, United Kingdom

*equal contribution
[#]corresponding authors

ABSTRACT

Integrins form focal adhesions (FAs) at the cell edge and fibrillar adhesions (FBs) located centrally, with both serving as a link to the actin cytoskeleton. Talins 1 and 2, key mechanosensitive proteins, are not functionally redundant. Talin1 is essential to FAs, while talin2 is found in large FAs and FBs. KANK (kidney ankyrin repeat-containing) family proteins regulate adhesion dynamics, with KANK2 binding both talins in FAs and localizing to FBs where only talin2 is present. Previously, we showed in melanoma cell line MDA-MB-435S that talin2 within integrin αVβ5 FAs interacts with KANK2 to regulate actin-microtubule (MT) dynamics, and knocking down either protein reduces cell migration. Here, we demonstrate that RPMI-7951 melanoma cells also use integrin αVβ5 FAs for adhesion but additionally form integrin α5β1 FBs, and that KANK2 and talin2 are present in both structures. KANK2 functionally interacts with talin1 to maintain FAs, and with talin2 to regulate their dynamics. KANK2 within FBs regulates cell migration. This was demonstrated upon KANK2 knockdown that mirrors integrin α5 knockdown, increasing migration *via* MTs. Overall, our study highlights the distinct roles of KANK2 and talin2 in different adhesion structures, influencing melanoma cell migration.

INTRODUCTION

Integrins are transmembrane cell surface proteins consisting of α and β subunits that combine to form 24 distinct heterodimers, enabling cell-to-cell or cell-to-extracellular matrix (ECM) connections (Green and Brown, 2019). Integrin heterodimer binding of ECM ligands results in the formation of several functionally and structurally different classes of integrin-based adhesions. These include short-lived peripheral nascent adhesions, which mature into focal adhesions (FAs) and further, centrally located, elongated fibrillar adhesions (FBs), which all serve as a link to the actin cytoskeleton (Burridge and Guilluy, 2016). Additionally, there are hemidesmosomes, which link to intermediate filaments (Walko et al., 2015), and reticular adhesions (RAs), which are not associated to the cytoskeleton (Lock et al., 2018).

Integrins are involved in the metastatic cascade and have been found to be responsible for intrinsic and acquired therapy resistance. Therefore, targeting integrins, or more specifically the signal transduction *via* integrin adhesion complexes (IACs), is a promising therapeutic opportunity to reduce tumor metastasis and overcome therapeutic resistance (Pang et al., 2023). However, despite highly encouraging preclinical data, targeting IACs in clinical trials has so far failed (Bergonzini et al., 2022, Samarzija et al., 2020). Therefore, further work is required not only to understand the role of different types of adhesions, their turnover and the relationships between adhesion structures, but also to unlock their therapeutic potential.

FAs are the most extensively studied IACs that convert extracellular chemical and mechanical cues into biochemical signals (Geiger and Yamada, 2011, Winograd-Katz et al., 2014). In culture, cells form FAs in order to adhere to their substrate. FAs link integrin heterodimers bound to ECM outside the cell and the actomyosin network inside the cell, acting *via* a range of adaptor proteins (Yamaguchi and Knaut, 2022, Mishra and Manavathi, 2021). FBs develop from mature FAs and have a role in promoting fibronectin remodeling (Zamir et al., 2000). They are

larger than FAs, with a dissimilar composition, and are located in the center of the migrating cell (Katz et al., 2000, Pankov et al., 2000). There are multiple integrin heterodimers commonly associated with FAs (e.g. αVβ3, αVβ5, α5β1, α3β1 and others) while integrin α5β1 is primarily involved in forming FBs (Conway and Jacquemet, 2019). In contrast to FAs and FBs, RAs represent a specialized, actin-independent adhesions mediated by integrin αVβ5. They are distinct from other adhesion types due to their lack of cytoskeletal connections and their high stability, making them uniquely suited for signaling and maintaining cell-ECM adhesion in situations where cytoskeletal connections are not required, such as cell division (Lock et al., 2018, Zuidema et al., 2018, Zuidema et al., 2020, Baschieri et al., 2018, Zuidema et al., 2022, Alfonzo-Mendez et al., 2022).

Talins are key cytoplasmic mechanosensitive proteins mediating binding of integrin adhesions to the ECM (Klapholz and Brown, 2017). There are two different isoforms of talins, talin1 and talin2. Although talin1 and talin2 share 76% protein sequence identity (88% similarity), they are not functionally redundant, and the differences between the two isoforms are not fully understood (Qi et al., 2016). Talin1 forms the core of IAC, increasing the affinity of integrin for ligands (integrin activation) and mediating the mechanosensitive link to actin (del Rio et al., 2009, Goult et al., 2021), while talin2 has been relatively less studied. Talins also coordinate microtubule (MT) recruitment to adhesion sites *via* interaction with KANK (kidney ankyrin repeat-containing) proteins, members of the cortical microtubule stabilizing complex (CMSC) (Bouchet et al., 2016, Goult et al., 2018, Klapholz and Brown, 2017, Sun et al., 2016, Loncaric et al., 2023).

KANK family proteins are evolutionarily conserved and consist of four paralogs (KANK1–4) due to gene expansion and diversification. KANK1 (around 170 kDa) is mainly found in epithelial, while KANK2 (around 120 kDa) in mesenchymal cells (Chen et al., 2018). KANK1 and 2 localize to the rims of mature integrin-containing FAs, termed the FA belt and adjacent regions. The CMSC, recruited upon talin-KANK2 interaction, stabilizes MTs in the vicinity of adhesions and regulates actin-MT crosstalk (Bouchet et al., 2016, van der Vaart et al., 2013). The uncoupling of FAs and CMSCs leads to the release of the RhoA GEF ARHGEF2 / GEF-H1 from MTs that in turn results in increased RhoA-mediated actomyosin contractility, reinforcement of the stress fiber-associated FAs and decreased FA turnover (Rafiq et al., 2019). Other possible localization of KANK2, with no reports indicating similar localization for KANK1, is in centrally positioned FBs. KANK2 in FAs binds talin in the vicinity of F-actin binding site 2 (ABS2) and destabilizes the talin-F-actin linkage that leads to slippage of integrin ligand bonds and adhesion sliding in the centrally positioned FBs (Sun et al., 2016).

A discrepancy in how KANK proteins affect cell migration and sensitivity to antitumor agents has been observed (reviewed in (Tadijan et al., 2021)). It is also not clear which talin isoform binds which KANK paralogue within the cell. While in HeLa cells Bouchet et al. (Bouchet et al., 2016) showed that talin1 binds KANK1, we have recently showed that KANK2 and talin2 functionally interact in the melanoma cell line MDA-MB-435S thus enabling the actin-MT crosstalk important for both sensitivity to MT poisons and cell migration (Loncaric et al., 2023).

Here, we present an analysis of IACs in the melanoma cell line RPMI-7951 cultivated in long-term culture. Our study explores the localization and roles of KANK2 and talin2, and demonstrates that both are part of integrin αVβ5 and α5β1-positive adhesions. In FAs, KANK2 functionally interacts (i) with talin1 to maintain FA, and (ii) with talin2 to regulate their dynamics. Our data also emphasize that KANK2 localized within FBs regulates cell migration *via* MTs.

MATERIALS AND METHODS

Cell Culture

The human melanoma cell line RPMI-7951 was obtained from the American Type Culture Collection (ATCC). Cells were grown on uncoated cell culture plates in DMEM (Invitrogen) supplemented with 10% (v/v) FBS (Invitrogen) (DMEM-FBS) at 37°C with 5% CO2 (v/v) in a humidified atmosphere.

Transient siRNA Transfection

For transient siRNA transfection, cells (3.7×10^4, 5×10^5 or 1×10^6) were plated in 24-well, 6-well cell culture plates or 10 cm diameter Petri dishes to achieve 60–80% confluence after 24 hours. Cells were transfected 24 hours later, using Lipofectamine RNAiMax (13778150, Thermo Fisher Scientific), with 25 nM of control (Silencer™ Select Negative Control No. 1 siRNA, Ambion), gene-specific siRNA for ITGAV (s7568, Ambion), ITGA5 (s7547, Ambion), ITGB5 (s7591, Ambion) or gene-specific siRNA for KANK2 (target sequence: ATGTCAACGTGCAAGATGA), TLN1 (target sequence: TGAATGTCCTGTCAACTGCTG) or TLN2 (target sequence: TTTCGTTTTCATCTACTCCTT) (Loncaric et al., 2023), all purchased from Sigma. Knockdown was

validated by SDS-PAGE and western blot (WB) using specific antibodies and matched labelled secondary antibodies, listed in Table S1.

Isolation of IACs

IACs were isolated from cells cultivated for 72 hours as described previously (Loncaric et al., 2023, Paradzik et al., 2020, Jones et al., 2015). Briefly, cells were washed with DMEM-HEPES and incubated with Wang and Richard's reagent (DTBP, 6 mM, Thermo Fisher Scientific) for 15 minutes. DTBP was quenched with 0.03M Tris-HCl (pH 8) and cells were lysed using modified RIPA buffer (50 mM Tris-HCl, pH 7.6; 150 mM NaCl; 5 mM disodium EDTA, pH 8; 1% (w/v) Triton X-100, 0.5% (w/v) SDS, 1% (w/v) sodium deoxycholate). Cell bodies were removed by high-pressure washing with tap water for 10 seconds and remaining adhesion complexes were collected by scraping into adhesion recovery solution (125 mM Tris-HCl, pH 6.8; 1% (w/v) SDS; 150 mM dithiothreitol). Samples containing isolated IACs were acetone-precipitated and further processed for Mass Spectrometry (MS) or Western Blotting (Robertson et al., 2015).

Sample Preparation for Mass Spectrometry and Data Analysis

Samples (prepared in triplicates) were processed as previously described (Jones et al., 2015, Paradzik et al., 2020) and analysed using an UltiMate R 3000 Rapid Separation LC (RSLC, United States) coupled to an Orbitrap Elite mass detector (Thermo Fisher Scientific, United States) with electrospray ionization. Peptide mixtures were eluted over 44 min using a gradient of 92% of solution A (0.1% formic acid in water) and 8% up to 33% of solution B (0.1% formic acid in acetonitrile). Solvent flow was set to 300 nL per minute. Protein identification was performed by searching data against the human SwissProt database (version 2018_01) using Mascot (Matrix science, version 2.5.1). Fragment ion tolerance was set to 0.50 Da, while parent ion tolerance was 5 PPM. Scaffold (Proteome software) was used to further refine protein identification. Protein (99.9%) and peptide (95%) probabilities were assigned using the Protein Prophet algorithm (Nesvizhskii et al., 2003) as incorporated by Scaffold including a minimum of four unique peptides per each protein. Data have been deposited in the ProteomeXchange Consortium (Deutsch et al., 2023) (dataset ID: PXD064756) via the PRIDE repository (Perez-Riverol et al., 2025).

Protein-protein Interaction Network Formation, Functional Enrichment, Gene Ontology Analysis, and MS Data Visualization

Human protein–protein interactions (PPIs) were loaded from STRING database, using stringApp (confidence score cut-off = 0.40, maximum additional interactors = 0) (Doncheva et al., 2019) for Cytoscape software (version 3.7.1) (Shannon et al., 2003). Functional annotation was performed using the Database for annotation, visualization and integrated discovery (DAVID), version 6.8 (Huang da et al., 2009a, Huang da et al., 2009b) and Panther GO database (Thomas et al., 2003). Functional enrichment analysis was carried out using the DAVID_CC subontology list (Benjamini–Hochberg corrected P-value < 0.05, EASE score < 0.1, at least four identified proteins). To summarize gene ontology (GO) terms and visualize them in a similarity-based space, the REVIGO tool was used with the following parameters: comparison of corrected P-values related to GO terms, allowed similarity set to small (0.5), and the Resnik-normalized semantic similarity measure (Supek et al., 2011). Differential protein expression analysis between RPMI-7951 si(-) and RPMI-7951 si(αV) datasets was performed using the QSpec spectral counter tool (Choi et al., 2008). A volcano plot was generated in GraphPad Prism to visualize differentially expressed proteins, using a fold-change threshold of >1.5 (RPMI-7951 si(-) vs. RPMI-7951 si(αV)) and a -log(FDR) >1. Fold changes were calculated based on QSpec output values.

Cell Survival Analysis

MTT (3-((4,5-dimethylthiazol-2-yl)-2,5- diphenyltetrazolium bromide) (Millipore) assay was used to determine sensitivity of cells to paclitaxel (PTX, Sigma-Aldrich). Briefly, 24 hours after seeding in 96-well tissue culture plates (1–1.2 × 10^4 cells/well) cells were treated with different concentrations of PTX. Seventy-two hours later, the absorbance of MTT-formazan product dissolved in DMSO was measured with a microplate reader (Awareness Technology, Inc.) at 600 nm. Absorbance is proportional to the number of viable cells.

Cell Migration

Serum-starved (24 hours) cells (8 × 10^4) were placed in Transwell Cell Culture Inserts (pore size, 8 µm) (Corning) in DMEM containing 0.1% (w/v) BSA) and left to migrate toward 10% (v/v) FBS in DMEM as a chemoattractant. After 22 hours, cells that remained on the upper side of the inserts were removed with cotton-tipped swabs. Inserts were fixed in 4% paraformaldehyde for 15 minutes followed by staining with 1% (w/v) crystal

violet in PBS for 90 minutes. Cells on the underside of the inserts were photographed using Olympus BX51TF microscope (five images/sample). The number of cells was determined using ImageJ software (Multi-point tool).

Confocal Microscopy

For immunofluorescence analysis (IF), cells were plated on coverslips in a 24-well plate (3.7×10^4 cells/well). After 48 hours, cells were fixed using ice-cold methanol for 10 minutes or 2% (v/v) paraformaldehyde for 12 minutes followed by permeabilization with 0.1% (v/v) Triton X-100 for 2 minutes, and incubated with specific primary antibodies for 1 hour, followed by conjugated secondary antibodies for 1 hour. The primary and secondary antibodies are listed in Table S1. Actin stress fibers were stained with rhodamine phalloidin (Cell Signaling Technology). Cells were mounted with DAPI Fluoromount-G (SouthernBiotech). Fluorescence and respective Interference Reflection Microscopy (IRM) images were acquired using an inverted confocal microscope Leica TCS SP8 X (Leica Microsystems) with the HC PL APOCS2 63×/1.40 oil-immersion objective, zoom set at 2×. Images were analysed using LAS X software 3.1.1 (Leica Microsystems) and ImageJ (NIH, USA). For actin stress fibers quantification, only fibers that ended with FAs, marked by FA marker staining (analysed but not presented in figures), were identified as stress fibers and quantified. For MT quantification, only MTs within 5 µm from the cell edge (identified through IRM images) were quantified. All images were taken with the focus adjusted to the adhesion sites of cells at the upper surface of glass coverslip.

Proximity ligation assay

Proximity ligation assay (PLA), using Duolink® PLA technology (Alam, 2018), was done according to manufacturer's instructions. Briefly, cells seeded on coverslips for 48 hours were fixed, blocked and incubated with selected primary antibodies for 1 hour at +37 °C in a preheated humidity chamber. Primary antibodies are listed in Table S1. Following washing, coverslips are incubated in secondary antibodies conjugated to proprietary oligonucleotide arms (Navenibodies) for 1 hour. Incubation with specific enzymes enables the formation and amplification of a DNA circle in the spots of protein proximity. Fluorescent dots, generated by binding of fluorescently labelled probes, were visualized using an inverted confocal microscope (Leica TCS SP8 X, Leica Microsystems) with the HC PL APOCS2 63×/1.40 oil-immersion objective, zoom set at 2×. Images were analysed using LAS X software 3.1.1 (Leica Microsystems) and ImageJ (NIH, USA).

Statistical Analysis

GraphPad Prism version 9.0.0 (GraphPad Software) was used to analyse data. Data obtained from IF, PLA and migration assay were analysed by one-way analysis of variance (ANOVA) with Dunnett's multiple comparison or by unpaired Welch's t-test, and expressed as histograms depicting mean ± standard deviation (SD); violin plots or scatter plots with marked median. Data obtained from MTT experiments were analysed by two-way ANOVA with Šídák's multiple comparisons test, with a single pooled variance and expressed as mean ± SD. ns denotes not significant; * denotes $p < 0.05$; ** denotes $p < 0.01$; *** denotes $p < 0.001$; **** denotes $p < 0.0001$.

RESULTS

Melanoma cell line RPMI-7951 primarily utilizes integrin heterodimer αVβ5 for adhesion

IACs, together with secreted ECM proteins, were isolated from RPMI-7951 melanoma cells grown for 72 hours as described previously (Paradzik et al., 2020, Loncaric et al., 2023). The optimal crosslinking duration was determined based on intracellular IAC components (liprin β1, FAK and paxillin) (Fig S1, S5). MS analysis identified 624 proteins, of which 45 are components of the consensus adhesome and 388 of the meta adhesome (Horton et al., 2015, Horton et al., 2016) (Table S2.1).

The adhesome of RPMI-7951 cells contained three integrin receptor subunits: αV, β5 and β1. The most abundant integrin subunits were αV and β5, suggesting that these cells primarily use αVβ5 and possibly αVβ1 for adhesion in long term 2D culture. α5 was detected, but at very low levels, suggesting that these cells may also express α5β1 (Table S2.1).

PPI network of the identified proteins indicated that the majority of identified proteins were ECM proteins and actin-binding proteins (Fig. 1A; Table S2.2). Proteins reported to bind MTs, intermediate filament related proteins, enzymes, HSP proteins and nuclear proteins were also identified. GO enrichment analysis was performed using DAVID (Huang da et al., 2009a, Huang da et al., 2009b) and proteins were assigned to functional groups and visualized using REVIGO (Supek et al., 2011). Analysis indicated a significant enrichment of GO terms related to ECM, extracellular exosome and FA (Fig.1B).

Integrin αVβ5-induced interaction networks

To determine which proteins were found in αVβ5-containing adhesions, transient knockdown of integrin subunit αV was performed and IAC composition was compared to control siRNA treatment using QSpec/QProt (Choi et al., 2008). Differences were visualized using a volcano plot (Fig.1C). αV knockdown removed virtually all αVβ5 from the cell surface, but did not alter β1 levels (Table S2.3), indicating that RPMI-7951 cells use other alpha subunit(s), possibly α5, to pair with β1. A volcano plot, displaying proteins whose abundance was different in RPMI-7951 cells transfected with integrin αV-specific siRNA compared to control siRNA (Fig.1C), identified key components of integrin αVβ5 IACs dependent on αV. The expression of 164 proteins was decreased by αV knockdown (Table S2.3).

Proteins that were elevated following integrin αV knockdown included slit homolog 2 protein (SLIT2), peroxidasin homolog (PXDN), tenascin C (TNC) and transforming growth factor-β-induced protein ig-h3 (TGFBI). DAVID analysis connected most of the proteins with extracellular space, ECM, extracellular exosome, proteinaceous extracellular matrix and membrane (Fig 1D, Table S2.3).

Proteins detected at lower levels upon integrin αV knockdown and detected by high number of spectra (Table S2.3) were actin-binding adhesome proteins (plectin, vinculin, talins 1 and 2, α-actinins 1 and 4, filamin A and B, PDLIM7 and PDLIM5), non-muscle myosins 9 and 10 (MYH9 and MYH10), zyxin (ZYX), ezrin (EZR), moesin (MSN), tensin 3 (TNS3), tropomyosin 3 isoform 1 (TPM3), palladin (PALLD) and caldesmon 1 (CALD1). Actin (ACTB), which was identified with a very high number of spectra, was also greatly reduced upon integrin αV knockdown. Furthermore, the levels of Ras GTPase-activating-like protein 1 (IQGAP1) and integrin linked kinase (ILK), which have been identified in consensus adhesome, were reduced (Horton et al., 2015). DAVID analysis connected most of the proteins with FAs, cell-cell adherens junctions, extracellular exosome, stress fibers and actin cytoskeleton (Fig 1D, Table S2.3). Selected MS results were confirmed by WB and/or IF (for plectin, talin1, talin2, vinculin, filamin A and B, α-actinins 1 and 4, IQGAP1) (Fig. S2A, C, S6). It has to be noted that in the adhesome we found TNS3. TNS3, together with TNS1 and TNS2, are found in FAs and FBs in fibroblasts, although to different degrees. TNS2 is localized mainly in FAs, while TNS3 is mostly found in FBs, and TNS1 is found in both (Clark et al., 2010). Our data, which show the presence of integrin α5 and β1, albeit in small number of spectra, and TNS3, support the possibility that RPMI-7951 cells, under long term growth conditions, may contain FBs.

Finally, reduced abundance of a few proteins that are not recognized as adhesome proteins was found. These included the chloride intracellular channel 1 (CLIC1) which was recently identified to recruit PIP5K1A/C to the leading edge of the plasma membrane, to generate a PIP2-rich microdomain and to activate talin (Peng et al., 2021).

Differential role of KANK2 in PTX sensitivity and migration in two melanoma cell lines, MDA-MB-435S and RPMI-7951

The CMSC proteins MACF1, liprin β1 and KANK2 were detected in RPMI-7951 cell IACs (Table S2.2), and were reduced upon transient integrin αV knockdown (Table S2.3). Other CMSC proteins, liprin α1 and ELKS were represented at a lower abundance while CLASPs (CLIP-associating proteins), kinesin family member 21A (KIF21A), plus-end tracking protein EB1 and LL5β were not found in RPMI-7951 cells either transfected with control or integrin αV siRNA (Table S2.3). The reduced abundance of liprin β1 and KANK2 was confirmed in RPMI-7951 cells transfected with integrin αV-specific siRNA using WB (Fig. S2B, S7).

Since we previously demonstrated that RPMI-7951 cells, similar to MDA-MB-435S cells, can be sensitized to PTX through integrin αV or β5 knockdown (Stojanovic et al., 2018), we investigated whether talin2 and KANK2 similarly influence actin-microtubule crosstalk and regulate PTX sensitivity (Paradzik et al., 2020, Loncaric et al., 2023). Talin2 knockdown in RPMI-7951 cells caused an increase in sensitivity as judged by the greater survival difference between control and talin2 knockdown cells in the presence of PTX (Fig. 2A). In contrast to MDA-MB-435S cells, where talin2 knockdown did not affect cell proliferation (Loncaric et al., 2023), the talin2 knockdown reduced RPMI-7951 cell proliferation (Fig. 2A). While KANK2 sensitizes MDA-MB-435S cells to PTX like talin2 (Loncaric et al., 2023), the transient KANK2 knockdown in RPMI-7951 cells had no effect on PTX sensitivity (Fig. 2B).

The differential roles of talin2 and KANK2 between these cell models was also evident in cell migration. In MDA-MB-435S cells, knockdown of either talin2 or KANK2 reduced cell migration (Loncaric et al., 2023). However, in RPMI-7951 cells, talin2 knockdown reduced cell migration, while KANK2 knockdown enhanced it (Fig. 2C). We conclude that KANK2 and talin2 play distinct roles in regulating PTX sensitivity and cell migration between two melanoma cell lines, MDA-MB-435S and RPMI-7951. Therefore, we decided to further investigate KANK2-containing adhesions in the RPMI-7951 cell line.

In RPMI-7951 cells talin1 is required for maintenance of integrin αVβ5 FAs while talin2 regulates FAs dynamics

The MS-proteomic data above demonstrate that integrin αV knockdown leads to the loss of talin1, talin2 and KANK2. To determine the localization of talin isoforms within integrin αVβ5 IACs, IF was employed. Figure 3A shows that both talin1 and talin2 colocalize with integrin β5. Talin1 colocalizes with integrin β5 at the cell edge in structures that resemble FAs. Integrin β5 colocalizes with talin2 both at the cell edge in FAs and in the center of the cell in structures which are talin1-negative, and according to localization and appearance represent RAs (Lock et al., 2018, Paradzik et al., 2020). Proximity of integrin β5 and talin2 was further confirmed using PLA (Fig. 3B). This is in line with our MS data that both talins are part of integrin αVβ5 IACs.

It has been shown that talin2 also localizes to FBs (Praekelt et al., 2012). Although RPMI-7951 cells were not seeded on the α5β1 ligand fibronectin, the MS analysis showed that cells excrete their own fibronectin and contain a low number of spectra for integrin heterodimers α5 and β1 in IACs isolates (Table S2.1). Talin2 was found in rod shaped αVβ5-negative structures (Fig 3A, second row magnified images), which may be FBs. In addition, in RPMI-7951 cells, the presence of α5-positive IACs that did not overlap with vinculin or integrin β5 was confirmed, indicating a structure different from FAs, i.e. FBs (Figure S3).

Next, RPMI-7951 cells were transfected with control, talin1- or talin2-specific siRNA and the location of both talins and integrin β5 was analysed. Knockdown of talin1 led to disruption of αVβ5 FAs and a reduction in cell size (Fig. 3C), supporting a key role for talin1 in maintaining FAs, as previously described by others (Goult et al., 2018). Upon talin1 knockdown, a simultaneous reduction of talin2-positive structures was observed. The remaining talin2 signal, which still colocalized with integrin β5, was found in the center of the cells and likely represents RAs (Fig. 3C, middle row), which are reported to be more stable and contain talin2 (Lock et al., 2018, Zuidema et al., 2018). In addition, after talin1 knockdown, talin2-positive and β5-negative rod-shaped structures reminiscent of FBs were observed (Fig. 3C, middle row, magnified images). Atherton et al. (Atherton et al., 2022) reported that the formation of FBs depends on force, but their maintenance is largely independent of intracellular tension. Therefore, it is possible that FBs remain upon talin1 knockdown. This conclusion was confirmed by analysing vinculin/talin1/talin2 expression in cells after talin1 knockdown where only RAs and FBs remain (Fig. S4). After talin2 knockdown, talin1-positive and integrin β5-positive FAs were still present, mostly at the cell edge and there was no visible effect on cell size (Fig. 3C, last row).

A quantitative assessment following talin1 knockdown, which notably reduced cell size (Fig 3D), demonstrated a significant reduction of number of talin2- or integrin β5-positive structures (Fig. 3E, first row), indicating the significant loss of integrin αVβ5 FAs. Simultaneously, the size of talin2-positive structures did not change (FBs and RAs) but the size of integrin β5-positive structures was greatly reduced (RAs) (Fig 3E, second row). As stated above, talin2 knockdown did not affect cell size (Fig. 3D) nor the presence of talin1-positive structures, however, their size increased (Fig. 3E), which indicates altered FAs dynamics. Additionally, talin2 knockdown reduced the number of integrin β5-positive structures without changing their size, which could indicate the reduction of number of structures other than integrin αVβ5 FAs, likely RAs (Fig. 3E). Indeed, analysis of the levels of RA components Numb and AP2 in IAC samples following talin2 knockdown and cytochalasin D treatment revealed their reduced levels (Rac et al., 2025).

In RPMI-7951 cells talin1 localizes with KANK2 predominantly at the cell edge while talin2 and KANK2 localize predominantly in the cell center

A key question was which talin isoform colocalizes with KANK2 in RPMI-7951 cells. Therefore, IF and PLA analysis of talin1, talin2 and KANK2 was performed. KANK2 was present in talin1- and talin2-positive structures at the cell edge (FAs) (Fig. 4A). The analysis of KANK2 proximity to talin1 also showed that they are predominantly located at the cell edge (Fig. 4B, C). KANK2 was also found in the central part of the cell where it colocalized mostly with talin2 but not with talin1, thus indicating structures different from FAs (Fig. 4A). Talin2-KANK2 proximity analysis showed the majority of positive signals located in the cell center (Fig. 4B, C).

RPMI-7951 cells were then transfected with control, talin1- or talin2-specific siRNA and the location of both talins and KANK2 was analysed. Knockdown of talin1 reduced the number and size of KANK2-positive structures (Fig. 4D, E). Since the knockdown of talin1 disrupts FAs and reduces the number of talin2-positive structures (Fig. 3C, E), the remaining KANK2-structures which colocalize with talin2 (Fig. 4D) are either (Rac et al., 2025) or FB (Atherton et al., 2022).

As before (Fig. 3C, E), the talin2 knockdown did not affect the number of talin1-positive structures but enhanced their size indicating alteration of FA dynamics. The knockdown of talin2 does not exhibit the same effect on KANK2-positive structures, as it does not alter their number or size (Fig. 4D, E). This does not imply that the knockdown of talin2 has no effect on KANK2 function. In fact, we previously demonstrated in MDA-MB-435S

cells that disrupting the talin2-KANK2 interaction through talin2 knockdown disconnects FAs from CMSCs. Nevertheless, this disruption does not impact the localization of KANK2 (Loncaric et al., 2023).

In RPMI-7951 cells KANK2 is part of all three adhesions: FAs, RAs and FBs

As previously emphasized, KANK2 is localized in talin1-positive adhesions at the cell edge but the majority of KANK2 is localized in the central region of the cell, where it colocalizes with talin2 but not talin1 (Fig. 4). We hypothesized that these central structures are α5β1 FBs and αVβ5 RAs. Our new data identified KANK2 within αVβ5 RAs (Rac et al., 2025). Next, to determine whether KANK2 localizes to FBs, the colocalization of integrin α5 and KANK2 was analysed. The results demonstrated that they indeed predominantly colocalize in the central part of the cell within rod-shaped structures i.e. FBs (Fig. 5A). The proximity between integrin α5 and KANK2 was further confirmed through PLA (Fig. 5B). Therefore, in addition to being in FAs and RAs, KANK2 is also part of FBs.

To analyse how a reduction of FBs affects other IACs, RPMI-7951 cells were transfected with control- or integrin α5-specific siRNA and the localization of talin1, talin2 and KANK2 was analysed. The knockdown of integrin α5 did not affect cell size (Fig. 5C, E), the number of talin1-, talin2-, or KANK2-positive structures, or the size of talin1-positive structures (FAs) (Fig. 5C, D). However, the size of talin2-positive structures increased, while size of KANK2-positive structures decreased (Fig. 5C, D), indicating a change in the dynamics of talin2- and KANK2-positive adhesions. The fact that FAs, FBs and RAs contain talin2 and KANK2 suggest that there is a crosstalk between FBs, FAs and/or RAs.

In RPMI-7951 cells KANK2-talin1 functional interaction is required for FA maintenance while KANK2-talin2 functional interaction regulates FA dynamics

Published studies (Atherton et al., 2022, Loncaric et al., 2023, Lock et al., 2018), our new data (Rac et al., 2025) combined with our own findings presented here (Fig. 3A-C; Fig. 4A, B; Fig. 5A, B) demonstrate that KANK2 and talin2 are part of FAs, RAs and FBs. Since we have shown above that talin1 regulates FA maintenance while talin2 affects FA dynamics, we aimed to determine the role of KANK2 in these events.

The knockdown of KANK2 reduced cell size (Fig. 5C, E) and the number of talin1-positive structures, but increased their size indicating change in the dynamics of FAs formed by either integrins αVβ5 or α5β1 (Fig. 5C, D). KANK2 knockdown also increased the size of α5-positive, but not β5-positive, structures (Fig. 6A-D), implying altered dynamics of α5β1 FA and/or FBs. However, this does not rule out the possibility that KANK2 knockdown influences αVβ5-positive adhesion dynamics, as αVβ5 forms FA and RAs which are very different in size, therefore overall changes in size may not be easily detected.

The reduction in the number of FAs after KANK2 knockdown (according to decreased number of talin1-positive structures) aligns with the observed reduction in cell size (Fig. 5C, E), which was previously also noted after talin1 knockdown (Fig. 3D). Since talin1 knockdown reduces talin2-positive structures (Fig. 3C, E), it was expected that KANK2 knockdown, which reduces talin1-positive structures, would also reduce the number of talin2-positive structures; indeed, this was the case (Fig. 5C, D). In conclusion, KANK2 knockdown mimics the effect of talin1 knockdown which indicates that the functional interaction between KANK2 and talin1 is necessary for FA maintenance. The knockdown of KANK2 mimics the impact of talin2 knockdown on the size of talin1-positive structures (increased size), suggesting that KANK2-talin2 functional interaction affects FA dynamics. Since talin2 knockdown only increases the size of talin1-positive structures (Fig. 3C, E) and doesn't affect either number or size of α5- (data not shown) or β5-positive structures (Fig. 3C, E), we cannot conclude in which FAs KANK2-talin2 functionally interact.

Talin2-KANK2 are in proximity in FAs, RAs and FBs

Next, PLA was employed to analyse talin2-KANK2 colocalization following integrin α5 or β5 knockdown. We hypothesized that we would observe a difference in distribution (cell edge vs cell center) as a consequence of loss of either FAs and RAs (integrin β5 knockdown) or integrin α5 FAs and FBs (integrin α5 knockdown). The distribution (percentage of talin2-KANK2-positive PLA signals at the cell edge or cell center) in cells transfected with control siRNA showed preferential location of talin2-KANK2-positive PLA signals in the cell center. After integrin α5 knockdown a small reduction in talin2-KANK2-positive PLA signals was observed in the cell center and a slight increase at the cell edge (Fig. 6E, F). This is in line with a reduction of FBs. After β5 knockdown, the percentage of talin2-KANK2-positive PLA signals at the cell edge and cell center changed even more, i.e. a strong reduction of signal in the cell center and increase at the cell edge were observed (Fig. 6E, F). This is in line with a

reduction of αVβ5 FA and RA, leaving only α5-positive FAs and FBs. In summary, talin2-KANK2 are in proximity to each other in FAs, RAs and FBs.

Loss of integrin α5 mimics the effect of KANK2 and increases cell migration

Since we found that KANK2 is located in FBs and that KANK2 knockdown increases migration, we hypothesized that α5 knockdown could mimic the effect of KANK2. Indeed, integrin α5 knockdown increased cell migration (Fig. 7A, B). To support the conclusion that increased migration is the consequence of reduced KANK2 from FBs and not αVβ5 FAs or RAs, migration was analysed after β5 knockdown and showed that it had the opposite effect, i.e. reduction of migration (Fig. 7A, B). Migration depends on the cytoskeleton, especially actin and MTs (Schmidt and Stehbens, 2024). In MDA-MB-435S cells, in which KANK2 is located preferentially within αVβ5 FAs, the functional interaction between talin2 and KANK2 regulates actin-MT crosstalk and reduces migration. In addition, we reported that interruption of talin2-KANK2 crosstalk leads to increased levels of actin stress fibers and a denser MT network with less MT fibers at the cell edge (Loncaric et al., 2023). Therefore, actin and MT distribution was analysed after talin1, talin2, integrin α5 or KANK2 knockdown using IF (Fig. 7C). The only change in actin was following talin1 knockdown which completely disrupted actin stress fibers (Fig. 7C, D); however, analysis of MTs showed that KANK2 and integrin α5 knockdown led to a more compact appearance of the MT network, which was denser at the cell edge (Fig. 7C, E). Talin2 knockdown, which reduces cell migration (Fig. 2C), led to a lower amount of MTs at the cell edge, which is the opposite effect of KANK2 or α5 knockdown (Fig. 7C, E). In summary, loss of integrin α5 or KANK2 from FBs increases cell migration through changes in the MT cytoskeleton.

DISCUSSION

Metastasis remains the primary cause of mortality in melanoma patients (Arias-Mejias et al., 2020). Current treatment options, including targeted drug therapy and immunotherapy, are not universally effective, with some patients exhibiting resistance. Therefore, better understanding of metastatic melanoma is required for the development of effective treatments. Integrins αVβ5 and α5β1 have been identified as potential therapeutic targets (Pang et al., 2023, Arias-Mejias et al., 2020, Vogetseder et al., 2013, Doyle et al., 2022). However, clinical trials targeting integrins have thus far been unsuccessful (Arias-Mejias et al., 2020, O'Day et al., 2011, Ruffini et al., 2015) due to several possible reasons: (i) variable integrin expression, (ii) redundancy in integrin function, (iii) distinct roles of integrins at various disease stages, and (iv) sequestering of therapeutics by integrin-containing tumor-derived extracellular vesicles (Samarzija et al., 2020, Pang et al., 2023, Bergonzini et al., 2022). We hypothesize that targeting IACs, which act downstream of integrins, may provide a more consistent therapeutic outcome.

In two melanoma cell lines, MDA-MB-435S and RPMI-7951, we showed that integrin αV or β5 knockdown increases sensitivity to the MT poison PTX and reduces cell migration (Stojanovic et al., 2018). To better understand the composition of IACs and their connection to observed changes in cell migration and PTX sensitivity, we analysed the adhesome of the melanoma cell line MDA-MB-435S. Upon integrin αV knockdown we observed reduced abundance of the integrin downstream effectors, KANK2 and talin2 (Paradzik et al., 2020). These proteins functionally interact, and their individual knockdown mimics integrin αV or β5 knockdown, leading to increased PTX sensitivity and decreased cell migration (Loncaric et al., 2023).

Here we analysed the adhesome of RPMI-7951 cells and found that, in long term culture, these cells also preferentially use integrin αVβ5 for adhesion. However, we also found integrin subunits α5 and β1, which form α5β1 FAs and FBs, and confirmed their presence by IF. Integrin αV knockdown in RPMI-7951 cells reduced KANK2 and talin2 levels but only talin2 mimicked the effect of integrin αV or β5 knockdown on PTX sensitivity and migration. In contrast, KANK2 knockdown mirrored the effect of integrin α5 knockdown, increasing cell migration. This led us to further investigate talin2 and KANK2 localization in RPMI-7951 cell adhesions.

Another difference between MDA-MB-435S and RPMI-7951 cells was the impact of integrin αV knockdown in the expression of ECM proteins, specifically TNC and TGFβ1. In MDA-MB-435S cells, integrin αV knockdown slightly reduced the abundance of these proteins (Paradzik et al., 2020). In RPMI-7951 cells, however, integrin αV knockdown increased the abundance of both proteins. These data suggest a differential feedback loop where cells secrete more of the ECM components necessary to ensure a homeostatic adhesion when some key adhesion molecules are missing. Given that TNC and TGFβ1 are linked to melanoma invasion and metastasis (Nummela et al., 2012, Shao et al., 2015), this differential response highlights the complexity of integrin-mediated regulation in melanoma progression.

In RPMI-7951 cells, talin1 and talin2 colocalize with integrin β5 at the cell edge within FAs. Talin2 is also found in rod shaped αVβ5-negative structures (FBs) and αVβ5-positive structures in the cell center (RAs). Similar patterns were observed in MDA-MB-435S cells (Loncaric et al., 2023), with the key exception that these cells form much less, if any FBs (Rac et al., 2025).

The reasons for the different localization of talin1 and talin2 in cells remain unknown. Both talins bind to β-integrin cytoplasmic tails *via* their N-terminal FERM domains, but the talin2 has a slightly higher binding affinity than talin1 (Anthis et al., 2009, Anthis et al., 2010). In RPMI-7951 cells, talin1 is essential for FA formation, as its knockdown leads to FA disassembly, and a subsequent loss of talin2. In contrast, talin2 knockdown does not affect FA number (talin1-positive adhesions) but reduces the number of integrin β5-positive adhesions, later identified as RAs. While talin2 is a component of RAs, it is not essential for their formation (Lock et al., 2018, Rac et al., 2025). Integrin αVβ5 and talin2 found in RAs can also be recruited to FAs, a process enhanced by increased cellular tension (Zuidema et al., 2022). In both, MDA-MB-435S and RPMI-7951 cells, talin2 knockdown also increases FA size but only in MDA-MB-435S cell did it increase stress fiber formation (Loncaric et al., 2023). Since in RPMI-7951 talin2 knockdown increases the size of talin1-positive adhesions without affecting actin stress fibers, it is unclear whether the reduction of RAs is due to talin2 exiting RAs or from changes in cell tension, as indicated by FA increased size.

As mentioned earlier, talin2 knockdown increases the size of talin1-positive adhesions, indicating changes in adhesion dynamics. However, no increase in size of β5- or α5-positive adhesions was observed. We assume that knockdown of talin2 affects primarily β5-positive adhesions. This is because statistical analysis of β5-positive adhesion size, observed through IF, may be unreliable, as it includes both FAs and RAs. Nonetheless, the reduction of RAs was confirmed through IAC isolation and WB (Rac et al., 2025). Therefore, talin2 knockdown in RPMI-7951 cells likely increases the size of integrin β5-positive FAs.

In RPMI-7951, as in MDA-MB-435S cells (Loncaric et al., 2023), there was no compensation between talin1 and talin2. A similar lack of compensation between talins was observed in early embryonic development (Monkley et al., 2000, Monkley et al., 2011). However, in fibroblasts, talin2 can compensate for the loss of talin1 (Zhang et al., 2008), and in endothelial cells, which express only talin1, introduced talin2 can compensate for talin1 loss (Kopp et al., 2010).

In HeLa cells and the HaCaT keratinocyte cell line, talin1 binds to KANK1, triggering the formation of CMSC, which surrounds adhesion sites and regulates their formation and dynamics via MT-dependent signalling and trafficking (Bouchet et al., 2016). In fibroblasts, KANK2 localizes to both FAs and FBs, where it interacts with talin1, dynein light chain isoforms (Dynll1 and Dynll2) and liprin-β1 (Sun et al., 2016). Recently, the proximity of TNS3 (enriched in FBs) to both talin1 and 2 and KANK2 was demonstrated (Atherton et al., 2022). In MDA-MB-435S cells, KANK2 functionally interacts with talin2 within integrin αVβ5 FAs, playing a role in actin-MT dynamics (Loncaric et al., 2023).

Our results in RPMI-7951 cells suggests a link between KANK2 and talin1 in FAs. KANK2 knockdown mimics talin1 knockdown by reducing cell size. It also decreased the number of talin1-positive adhesions (FAs). Since talin1 is a main regulator of FA assembly, this reduction subsequently leads to decreased talin2 levels and enlarged FAs. Proximity analysis revealed that KANK2-talin1 positive PLA signals are predominantly located at the cell edge, where FAs are positioned. In contrast, KANK2-talin2 signals are located predominantly in the cell center, corresponding to the location of FBs and RAs. We tried to obtain additional evidence of which talin binds KANK2 using WB analysis of isolated IACs after talin2 knockdown. In MDA-MB-435S cells, talin2 knockdown significantly reduced cross-linked KANK2 levels, confirming its binding to talin2 (Loncaric et al., 2023). However, in RPMI-7951 cells, cross-linked KANK2 levels after talin2 knockdown remained inconclusive. The results obtained in MDA-MB-435S cells (Loncaric et al., 2023) were informative as these cells form FAs and RAs and do not contain FBs (Rac et al., 2025). However, in RPMI-7951 cells talin2 and KANK2 are present in all three types of adhesions, FAs, FBs and RAs. The absence of KANK2 reduction in IAC isolates in RPMI-7951 cells may be reflection of the differences in adhesion composition rather than a lack of interaction with talin2.

In RPMI-7951 FBs, KANK2 is preferentially linked to talin2, as demonstrated by talin2-KANK2 PLA analysis following integrin α5 or β5 knockdown. Upon integrin α5 knockdown, the percentage of talin2-KANK2 PLA signals in the cell center decreases, consistent with a reduction in FBs. Following β5 knockdown, the percentage of talin2-KANK2 PLA signals at the cell edge and cell center changes compared to control, leaving only α5-positive FAs and FBs. Since the precise distribution of talin2-KANK2 levels in FAs and RAs remain unknown, the observed changes in the cell center and at the cell edge indicate that talin2 and KANK2 are present in both types of β5-positive adhesions. Collectively, our findings indicate that in RPMI-7951 cells, KANK2 associates with talin1 in FAs and with talin2 in all three adhesion types - FAs, RAs and FBs. However, KANK2 shows a clear preference for talin1 in FAs, whereas in FBs and RAs, which lack talin1, KANK2 is linked to talin2.

The factors determining why KANK2 interacts with talin1 or talin2 are not known. One possibility is that KANK proteins generally localize to the periphery of FAs (Sun et al., 2016, Bouchet et al., 2016). This suggests that FAs may initially form with talin1, while talin2 is later recruited to the outer rim, allowing KANK2 from CMSC to establish actin-MT crosstalk. In MDA-MB-435S cells, we hypothesized that talin1 is phosphorylated by CDK1 (Gough et al., 2021) and therefore has a low KANK binding affinity. It is unclear whether the situation is reversed in RPMI-7951 cells – where talin2 might be phosphorylated, leading KANK2 to favour talin1.

In both MDA-MB-435S and RPMI-7951 cells, integrin αV or β5 knockdown increases PTX sensitivity and reduces cell migration (Stojanovic et al., 2018). However, while KANK2 and talin2 knockdown in MDA-MB-435S cells mimic this effect (Loncaric et al., 2023, Paradzik et al., 2020), we found that KANK2 knockdown in RPMI-7951 cells has a different outcome. It does not affect PTX sensitivity and unexpectedly increases cell migration. This finding aligns with studies in fibroblasts, where adhesion sliding and formation of FBs containing KANK2 was linked to reduced migration speed (Sun et al., 2016). It also supports our observation that KANK2 knockdown mimics the integrin α5 knockdown, leading to increased migration.

In RPMI-7951 cells KANK2 knockdown increased the size of α5- and talin1-positive structures indicating altered α5β1 FA and/or FBs dynamics. It also mimicked integrin α5 knockdown by increasing cell migration and altering MTs, specifically increasing the percentage of MTs at the cell edge. This contrasts with findings in MDA-MB-435S cells, where talin2 or KANK2 knockdown from αVβ5 FAs disrupted actin-MT crosstalk, leading to decreased MT presence at the cell edge (Loncaric et al., 2023). Talin2 knockdown in RPMI-7951 cells, despite colocalizing with KANK2 and integrin α5 FBs, decreased the percentage of MTs at the cell edge and mimicked integrin αV or β5 knockdown by reducing cell migration. MT destabilization promotes the relocalization of integrin β5 from flat clathrin lattices, which are interspersed within RAs (Lukas et al., 2025), to FAs through tension modulation (Zuidema et al., 2022). Therefore, our study highlights the fact that in RPMI-7951 cells talin2, KANK2 and integrin α5 knockdown influence MTs. It remains unclear whether these effects are a result of direct connection between FBs and MTs (e.g. through CMSCs) or crosstalk between different adhesion structures. Further investigation is needed to clarify how FBs interact with MTs.

After integrin α5 knockdown, talin2-positive structures increased in size, while size of KANK2-positive structures decreased. Since talin1- and β5-positive structures remained unaffected, it is difficult to hypothesize which adhesions were impacted. However, since talin2 and KANK2 are present in all three adhesion structures FA, FB and RA, we conclude there is crosstalk between them. Indeed, it has been recently demonstrated that RAs are opposed by active integrin α5β1 (Hakanpaa et al., 2023).

In conclusion, the functional interactions between talin1, talin2 and KANK2 appear to be cell type-specific. However, our findings reveal that these interactions are influenced by their location within a specific adhesion structure. The factors guiding talin1/talin2 and KANK2 to particular adhesions remain unknown. To unlock the potential of integrins to be targets in metastatic melanoma, it is important to understand IAC composition and the role of individual components in different adhesions. Our study shows that KANK2 and talin2 are present in distinct adhesion structures and likely have different binding partners. Future studies should focus on identifying KANK2 and talin2 interactors both *in vitro* and *in vivo* to uncover new avenues for cancer treatment.

Data availability statement

The mass spectrometry proteomics data have been deposited to the ProteomeXchange Consortium via the PRIDE partner repository with the dataset identifier PXD064756. Other raw data supporting the conclusions of this article will be made available by the authors, without undue reservation, to any qualified researcher.

Author contributions

Material preparation, data collection and analysis were performed by [NS], [AR], [ML], [AT], [MP], [MA], and [AA-R]. [NS] and [AR] contributed equally to the experimental work. The first draft of the manuscript was written by [NS] and [AA-R], corrections were made by [AR], [ML], [JDH] and [MJH]. All authors read and approved the final manuscript. [NS] and [AA-R] equally contributed to the study conception and design.

Funding

This work was supported by the Croatian Science Foundation Project (Grant No IP-2019-04-1577 to AA-R), a Cancer Research UK Programme Grant to MJH (DRCRPG-100002) and an Academy of Medical Science Springboard award to JDH (SBF008\1094).

REFERENCES

ALAM, M. S. 2018. Proximity Ligation Assay (PLA). *Curr Protoc Immunol,* 123**,** e58.

ALFONZO-MENDEZ, M. A., SOCHACKI, K. A., STRUB, M. P. & TARASKA, J. W. 2022. Dual clathrin and integrin signaling systems regulate growth factor receptor activation. *Nat Commun,* 13**,** 905.

ANTHIS, N. J., WEGENER, K. L., CRITCHLEY, D. R. & CAMPBELL, I. D. 2010. Structural diversity in integrin/talin interactions. *Structure,* 18**,** 1654-66.

ANTHIS, N. J., WEGENER, K. L., YE, F., KIM, C., GOULT, B. T., LOWE, E. D., VAKONAKIS, I., BATE, N., CRITCHLEY, D. R., GINSBERG, M. H. & CAMPBELL, I. D. 2009. The structure of an integrin/talin complex reveals the basis of inside-out signal transduction. *EMBO J,* 28**,** 3623-32.

ARIAS-MEJIAS, S. M., WARDA, K. Y., QUATTROCCHI, E., ALONSO-QUINONES, H., SOMINIDI-DAMODARAN, S. & MEVES, A. 2020. The role of integrins in melanoma: a review. *Int J Dermatol,* 59**,** 525-534.

ATHERTON, P., KONSTANTINOU, R., NEO, S. P., WANG, E., BALLOI, E., PTUSHKINA, M., BENNETT, H., CLARK, K., GUNARATNE, J., CRITCHLEY, D., BARSUKOV, I., MANSER, E. & BALLESTREM, C. 2022. Tensin3 interaction with talin drives the formation of fibronectin-associated fibrillar adhesions. *J Cell Biol,* 221.

BASCHIERI, F., DAYOT, S., ELKHATIB, N., LY, N., CAPMANY, A., SCHAUER, K., BETZ, T., VIGNJEVIC, D. M., POINCLOUX, R. & MONTAGNAC, G. 2018. Frustrated endocytosis controls contractility-independent mechanotransduction at clathrin-coated structures. *Nat Commun,* 9**,** 3825.

BERGONZINI, C., KROESE, K., ZWEEMER, A. J. M. & DANEN, E. H. J. 2022. Targeting Integrins for Cancer Therapy - Disappointments and Opportunities. *Front Cell Dev Biol,* 10**,** 863850.

BOUCHET, B. P., GOUGH, R. E., AMMON, Y. C., VAN DE WILLIGE, D., POST, H., JACQUEMET, G., ALTELAAR, A. M., HECK, A. J., GOULT, B. T. & AKHMANOVA, A. 2016. Talin-KANK1 interaction controls the recruitment of cortical microtubule stabilizing complexes to focal adhesions. *Elife,* 5.

BURRIDGE, K. & GUILLUY, C. 2016. Focal adhesions, stress fibers and mechanical tension. *Exp Cell Res,* 343**,** 14-20.

CHEN, N. P., SUN, Z. & FASSLER, R. 2018. The Kank family proteins in adhesion dynamics. *Curr Opin Cell Biol,* 54**,** 130-136.

CHOI, H., FERMIN, D. & NESVIZHSKII, A. I. 2008. Significance analysis of spectral count data in label-free shotgun proteomics. *Mol Cell Proteomics,* 7**,** 2373-85.

CLARK, K., HOWE, J. D., PULLAR, C. E., GREEN, J. A., ARTYM, V. V., YAMADA, K. M. & CRITCHLEY, D. R. 2010. Tensin 2 modulates cell contractility in 3D collagen gels through the RhoGAP DLC1. *J Cell Biochem,* 109**,** 808-17.

CONWAY, J. R. W. & JACQUEMET, G. 2019. Cell matrix adhesion in cell migration. *Essays Biochem,* 63**,** 535-551.

DEL RIO, A., PEREZ-JIMENEZ, R., LIU, R., ROCA-CUSACHS, P., FERNANDEZ, J. M. & SHEETZ, M. P. 2009. Stretching single talin rod molecules activates vinculin binding. *Science,* 323**,** 638-41.

DEUTSCH, E. W., BANDEIRA, N., PEREZ-RIVEROL, Y., SHARMA, V., CARVER, J. J., MENDOZA, L., KUNDU, D. J., WANG, S., BANDLA, C., KAMATCHINATHAN, S., HEWAPATHIRANA, S., PULLMAN, B. S., WERTZ, J., SUN, Z., KAWANO, S., OKUDA, S., WATANABE, Y., MACLEAN, B., MACCOSS, M. J., ZHU, Y., ISHIHAMA, Y. & VIZCAINO, J. A. 2023. The ProteomeXchange consortium at 10 years: 2023 update. *Nucleic Acids Res,* 51**,** D1539-D1548.

DONCHEVA, N. T., MORRIS, J. H., GORODKIN, J. & JENSEN, L. J. 2019. Cytoscape StringApp: Network Analysis and Visualization of Proteomics Data. *J Proteome Res,* 18**,** 623-632.

DOYLE, A. D., NAZARI, S. S. & YAMADA, K. M. 2022. Cell-extracellular matrix dynamics. *Phys Biol,* 19.

GEIGER, B. & YAMADA, K. M. 2011. Molecular architecture and function of matrix adhesions. *Cold Spring Harb Perspect Biol,* 3.

GOUGH, R. E., JONES, M. C., ZACHARCHENKO, T., LE, S., YU, M., JACQUEMET, G., MUENCH, S. P., YAN, J., HUMPHRIES, J. D., JORGENSEN, C., HUMPHRIES, M. J. & GOULT, B. T. 2021. Talin mechanosensitivity is modulated by a direct interaction with cyclin-dependent kinase-1. *J Biol Chem,* 297**,** 100837.

GOULT, B. T., BROWN, N. H. & SCHWARTZ, M. A. 2021. Talin in mechanotransduction and mechanomemory at a glance. *J Cell Sci,* 134.

GOULT, B. T., YAN, J. & SCHWARTZ, M. A. 2018. Talin as a mechanosensitive signaling hub. *J Cell Biol,* 217**,** 3776-3784.

GREEN, H. J. & BROWN, N. H. 2019. Integrin intracellular machinery in action. *Exp Cell Res,* 378**,** 226-231.

HAKANPAA, L., ABOUELEZZ, A., LENAERTS, A. S., CULFA, S., ALGIE, M., BARLUND, J., KATAJISTO, P., MCMAHON, H. & ALMEIDA-SOUZA, L. 2023. Reticular adhesions are assembled at flat clathrin lattices and opposed by active integrin alpha5beta1. *J Cell Biol,* 222.

HORTON, E. R., BYRON, A., ASKARI, J. A., NG, D. H. J., MILLON-FREMILLON, A., ROBERTSON, J., KOPER, E. J., PAUL, N. R., WARWOOD, S., KNIGHT, D., HUMPHRIES, J. D. & HUMPHRIES, M. J. 2015. Definition of a consensus integrin adhesome and its dynamics during adhesion complex assembly and disassembly. *Nat Cell Biol,* 17**,** 1577-1587.

HORTON, E. R., HUMPHRIES, J. D., JAMES, J., JONES, M. C., ASKARI, J. A. & HUMPHRIES, M. J. 2016. The integrin adhesome network at a glance. *J Cell Sci,* 129**,** 4159-4163.

HUANG DA, W., SHERMAN, B. T. & LEMPICKI, R. A. 2009a. Bioinformatics enrichment tools: paths toward the comprehensive functional analysis of large gene lists. *Nucleic Acids Res,* 37**,** 1-13.

HUANG DA, W., SHERMAN, B. T. & LEMPICKI, R. A. 2009b. Systematic and integrative analysis of large gene lists using DAVID bioinformatics resources. *Nat Protoc,* 4**,** 44-57.

JONES, M. C., HUMPHRIES, J. D., BYRON, A., MILLON-FREMILLON, A., ROBERTSON, J., PAUL, N. R., NG, D. H. J., ASKARI, J. A. & HUMPHRIES, M. J. 2015. Isolation of integrin-based adhesion complexes. *Curr Protoc Cell Biol,* 66**,** 9 8 1-9 8 15.

KATZ, B. Z., ZAMIR, E., BERSHADSKY, A., KAM, Z., YAMADA, K. M. & GEIGER, B. 2000. Physical state of the extracellular matrix regulates the structure and molecular composition of cell-matrix adhesions. *Mol Biol Cell,* 11**,** 1047-60.

KLAPHOLZ, B. & BROWN, N. H. 2017. Talin - the master of integrin adhesions. *J Cell Sci,* 130**,** 2435-2446.

KOPP, P. M., BATE, N., HANSEN, T. M., BRINDLE, N. P. J., PRAEKELT, U., DEBRAND, E., COLEMAN, S., MAZZEO, D., GOULT, B. T., GINGRAS, A. R., PRITCHARD, C. A., CRITCHLEY, D. R. & MONKLEY, S. J. 2010. Studies on the morphology and spreading of human endothelial cells define key inter- and intramolecular interactions for talin1. *European Journal of Cell Biology,* 89**,** 661-673.

LOCK, J. G., JONES, M. C., ASKARI, J. A., GONG, X., ODDONE, A., OLOFSSON, H., GORANSSON, S., LAKADAMYALI, M., HUMPHRIES, M. J. & STROMBLAD, S. 2018. Reticular adhesions are a distinct class of cell-matrix adhesions that mediate attachment during mitosis. *Nat Cell Biol,* 20**,** 1290-1302.

LONCARIC, M., STOJANOVIC, N., RAC-JUSTAMENT, A., COOPMANS, K., MAJHEN, D., HUMPHRIES, J. D., HUMPHRIES, M. J. & AMBRIOVIC-RISTOV, A. 2023. Talin2 and KANK2 functionally interact to regulate microtubule dynamics, paclitaxel sensitivity and cell migration in the MDA-MB-435S melanoma cell line. *Cell Mol Biol Lett,* 28**,** 56.

MISHRA, Y. G. & MANAVATHI, B. 2021. Focal adhesion dynamics in cellular function and disease. *Cell Signal,* 85**,** 110046.

MONKLEY, S. J., KOSTOUROU, V., SPENCE, L., PETRICH, B., COLEMAN, S., GINSBERG, M. H., PRITCHARD, C. A. & CRITCHLEY, D. R. 2011. Endothelial cell talin1 is essential for embryonic angiogenesis. *Developmental Biology,* 349**,** 494-502.

MONKLEY, S. J., ZHOU, X. H., KINSTON, S. J., GIBLETT, S. M., HEMMINGS, L., PRIDDLE, H., BROWN, J. E., PRITCHARD, C. A., CRITCHLEY, D. R. & FASSLER, R. 2000. Disruption of the talin gene arrests mouse development at the gastrulation stage. *Dev Dyn,* 219**,** 560-74.

NESVIZHSKII, A. I., KELLER, A., KOLKER, E. & AEBERSOLD, R. 2003. A statistical model for identifying proteins by tandem mass spectrometry. *Anal Chem,* 75**,** 4646-58.

NUMMELA, P., LAMMI, J., SOIKKELI, J., SAKSELA, O., LAAKKONEN, P. & HÖLTTÄ, E. 2012. Transforming Growth Factor Beta-Induced (TGFBI) Is an Anti-Adhesive Protein Regulating the Invasive Growth of Melanoma Cells. *The American Journal of Pathology,* 180**,** 1663-1674.

O'DAY, S., PAVLICK, A., LOQUAI, C., LAWSON, D., GUTZMER, R., RICHARDS, J., SCHADENDORF, D., THOMPSON, J. A., GONZALEZ, R., TREFZER, U., MOHR, P., OTTENSMEIER, C., CHAO, D., ZHONG, B., DE BOER, C. J., UHLAR, C., MARSHALL, D., GORE, M. E., LANG, Z., HAIT, W., HO, P. & INVESTIGATORS, C. 2011. A randomised, phase II study of intetumumab, an anti-alphav-integrin mAb, alone and with dacarbazine in stage IV melanoma. *Br J Cancer,* 105**,** 346-52.

PANG, X., HE, X., QIU, Z., ZHANG, H., XIE, R., LIU, Z., GU, Y., ZHAO, N., XIANG, Q. & CUI, Y. 2023. Targeting integrin pathways: mechanisms and advances in therapy. *Signal Transduct Target Ther,* 8**,** 1.

PANKOV, R., CUKIERMAN, E., KATZ, B. Z., MATSUMOTO, K., LIN, D. C., LIN, S., HAHN, C. & YAMADA, K. M. 2000. Integrin dynamics and matrix assembly: tensin-dependent translocation of alpha(5)beta(1) integrins promotes early fibronectin fibrillogenesis. *J Cell Biol,* 148**,** 1075-90.

PARADZIK, M., HUMPHRIES, J. D., STOJANOVIC, N., NESTIC, D., MAJHEN, D., DEKANIC, A., SAMARZIJA, I., SEDDA, D., WEBER, I., HUMPHRIES, M. J. & AMBRIOVIC-RISTOV, A. 2020. KANK2 Links alphaVbeta5 Focal Adhesions to Microtubules and Regulates Sensitivity to Microtubule Poisons and Cell Migration. *Front Cell Dev Biol,* 8**,** 125.

PENG, J. M., LIN, S. H., YU, M. C. & HSIEH, S. Y. 2021. CLIC1 recruits PIP5K1A/C to induce cell-matrix adhesions for tumor metastasis. *J Clin Invest,* 131.

PEREZ-RIVEROL, Y., BANDLA, C., KUNDU, D. J., KAMATCHINATHAN, S., BAI, J., HEWAPATHIRANA, S., JOHN, N. S., PRAKASH, A., WALZER, M., WANG, S. & VIZCAINO, J. A. 2025. The PRIDE database at 20 years: 2025 update. *Nucleic Acids Res,* 53**,** D543-D553.

PRAEKELT, U., KOPP, P. M., REHM, K., LINDER, S., BATE, N., PATEL, B., DEBRAND, E., MANSO, A. M., ROSS, R. S., CONTI, F., ZHANG, M. Z., HARRIS, R. C., ZENT, R., CRITCHLEY, D. R. & MONKLEY, S. J. 2012. New isoform-specific monoclonal antibodies reveal different sub-cellular localisations for talin1 and talin2. *Eur J Cell Biol,* 91**,** 180-91.

QI, L., JAFARI, N., LI, X., CHEN, Z., LI, L., HYTONEN, V. P., GOULT, B. T., ZHAN, C. G. & HUANG, C. 2016. Talin2-mediated traction force drives matrix degradation and cell invasion. *J Cell Sci,* 129**,** 3661-3674.

RAC, A., LONCARIC, M., STOJANOVIC, N., FATIMA, M., RESETAR, M., HRSAK, D., HUMPHRIES, J. D., HUMPHRIES, M. J. & AMBRIOVIC-RISTOV, A. 2025. Regulation of reticular adhesions by KANK2 and talin2 in two melanoma cell lines. *bioRxiv***,** 2025.06.02.657402.

RAFIQ, N. B. M., NISHIMURA, Y., PLOTNIKOV, S. V., THIAGARAJAN, V., ZHANG, Z., SHI, S., NATARAJAN, M., VIASNOFF, V., KANCHANAWONG, P., JONES, G. E. & BERSHADSKY, A. D. 2019. Publisher Correction: A mechano-signalling network linking microtubules, myosin IIA filaments and integrin-based adhesions. *Nat Mater,* 18**,** 770.

ROBERTSON, J., JACQUEMET, G., BYRON, A., JONES, M. C., WARWOOD, S., SELLEY, J. N., KNIGHT, D., HUMPHRIES, J. D. & HUMPHRIES, M. J. 2015. Defining the phospho-adhesome through the phosphoproteomic analysis of integrin signalling. *Nat Commun,* 6**,** 6265.

RUFFINI, F., GRAZIANI, G., LEVATI, L., TENTORI, L., D'ATRI, S. & LACAL, P. M. 2015. Cilengitide downmodulates invasiveness and vasculogenic mimicry of neuropilin 1 expressing melanoma cells through the inhibition of alphavbeta5 integrin. *Int J Cancer,* 136**,** E545-58.

SAMARZIJA, I., DEKANIC, A., HUMPHRIES, J. D., PARADZIK, M., STOJANOVIC, N., HUMPHRIES, M. J. & AMBRIOVIC-RISTOV, A. 2020. Integrin Crosstalk Contributes to the Complexity of Signalling and Unpredictable Cancer Cell Fates. *Cancers (Basel),* 12.

SCHMIDT, C. J. & STEHBENS, S. J. 2024. Microtubule control of migration: Coordination in confinement. *Curr Opin Cell Biol,* 86**,** 102289.

SHANNON, P., MARKIEL, A., OZIER, O., BALIGA, N. S., WANG, J. T., RAMAGE, D., AMIN, N., SCHWIKOWSKI, B. & IDEKER, T. 2003. Cytoscape: a software environment for integrated models of biomolecular interaction networks. *Genome Res,* 13**,** 2498-504.

SHAO, H., KIRKWOOD, J. M. & WELLS, A. 2015. Tenascin-C Signaling in melanoma. *Cell Adh Migr,* 9**,** 125-30.

STOJANOVIC, N., DEKANIC, A., PARADZIK, M., MAJHEN, D., FERENCAK, K., RUSCIC, J., BARDAK, I., SUPINA, C., TOMICIC, M. T., CHRISTMANN, M., OSMAK, M. & AMBRIOVIC-RISTOV, A. 2018. Differential Effects of Integrin alphav Knockdown and Cilengitide on Sensitization of Triple-Negative Breast Cancer and Melanoma Cells to Microtubule Poisons. *Mol Pharmacol,* 94**,** 1334-1351.

SUN, Z., TSENG, H. Y., TAN, S., SENGER, F., KURZAWA, L., DEDDEN, D., MIZUNO, N., WASIK, A. A., THERY, M., DUNN, A. R. & FASSLER, R. 2016. Kank2 activates talin, reduces force transduction across integrins and induces central adhesion formation. *Nat Cell Biol,* 18**,** 941-53.

SUPEK, F., BOSNJAK, M., SKUNCA, N. & SMUC, T. 2011. REVIGO summarizes and visualizes long lists of gene ontology terms. *PLoS One,* 6**,** e21800.

TADIJAN, A., HUMPHRIES, J. D., SAMARZIJA, I., STOJANOVIC, N., ZHA, J., CULJAK, K., TOMIC, M., PARADZIK, M., NESTIC, D., KANG, H., HUMPHRIES, M. J. & AMBRIOVIC-RISTOV, A. 2021. The Tongue Squamous Carcinoma Cell Line Cal27 Primarily Employs Integrin alpha6beta4-Containing Type II Hemidesmosomes for Adhesion Which Contribute to Anticancer Drug Sensitivity. *Front Cell Dev Biol,* 9**,** 786758.

THOMAS, P. D., CAMPBELL, M. J., KEJARIWAL, A., MI, H., KARLAK, B., DAVERMAN, R., DIEMER, K., MURUGANUJAN, A. & NARECHANIA, A. 2003. PANTHER: a library of protein families and subfamilies indexed by function. *Genome Res,* 13**,** 2129-41.

VAN DER VAART, B., VAN RIEL, W. E., DOODHI, H., KEVENAAR, J. T., KATRUKHA, E. A., GUMY, L., BOUCHET, B. P., GRIGORIEV, I., SPANGLER, S. A., YU, K. L., WULF, P. S., WU, J., LANSBERGEN, G., VAN BATTUM, E. Y., PASTERKAMP, R. J., MIMORI-KIYOSUE, Y., DEMMERS, J., OLIERIC, N., MALY, I. V., HOOGENRAAD, C. C. & AKHMANOVA, A. 2013. CFEOM1-associated kinesin KIF21A is a cortical microtubule growth inhibitor. *Dev Cell,* 27**,** 145-160.

VOGETSEDER, A., THIES, S., INGOLD, B., ROTH, P., WELLER, M., SCHRAML, P., GOODMAN, S. L. & MOCH, H. 2013. alphav-Integrin isoform expression in primary human tumors and brain metastases. *Int J Cancer,* 133**,** 2362-71.

WALKO, G., CASTANON, M. J. & WICHE, G. 2015. Molecular architecture and function of the hemidesmosome. *Cell Tissue Res,* 360**,** 363-78.

WINOGRAD-KATZ, S. E., FASSLER, R., GEIGER, B. & LEGATE, K. R. 2014. The integrin adhesome: from genes and proteins to human disease. *Nat Rev Mol Cell Biol,* 15**,** 273-88.

YAMAGUCHI, N. & KNAUT, H. 2022. Focal adhesion-mediated cell anchoring and migration: from in vitro to in vivo. *Development,* 149.

ZAMIR, E., KATZ, M., POSEN, Y., EREZ, N., YAMADA, K. M., KATZ, B. Z., LIN, S., LIN, D. C., BERSHADSKY, A., KAM, Z. & GEIGER, B. 2000. Dynamics and segregation of cell-matrix adhesions in cultured fibroblasts. *Nat Cell Biol,* 2**,** 191-6.

ZHANG, X., JIANG, G., CAI, Y., MONKLEY, S. J., CRITCHLEY, D. R. & SHEETZ, M. P. 2008. Talin depletion reveals independence of initial cell spreading from integrin activation and traction. *Nat Cell Biol,* 10**,** 1062-8.

ZUIDEMA, A., WANG, W., KREFT, M., BLEIJERVELD, O. B., HOEKMAN, L., ARETZ, J., BOTTCHER, R. T., FASSLER, R. & SONNENBERG, A. 2022. Molecular determinants of alphaVbeta5 localization in flat clathrin lattices - role of alphaVbeta5 in cell adhesion and proliferation. *J Cell Sci,* 135.

ZUIDEMA, A., WANG, W., KREFT, M., TE MOLDER, L., HOEKMAN, L., BLEIJERVELD, O. B., NAHIDIAZAR, L., JANSSEN, H. & SONNENBERG, A. 2018. Mechanisms of integrin alphaVbeta5 clustering in flat clathrin lattices. *J Cell Sci,* 131.

ZUIDEMA, A., WANG, W. & SONNENBERG, A. 2020. Crosstalk between Cell Adhesion Complexes in Regulation of Mechanotransduction. *Bioessays,* 42**,** e2000119.

FIGURE LEGENDS

Fig. 1 MS analysis of IACs isolated from RPMI-7951 cells. (A) PPI network of proteins identified by MS in IACs isolated from RPMI-7951 cells. Shapes signify identified proteins and are labelled with gene symbols, arranged and coloured according to their functional group as indicated. **(B)** IACs isolated from RPMI-7951 are enriched with proteins connected to the ECM, extracellular exosome and FA. Proteins from (A) were assigned to functional groups using the DAVID GO database (GOTERM_CC_DIRECT) and visualized using the REVIGO tool, where p-values related to GO terms of cellular components were represented by the colour bar and size of the circle. Statistically significant GO terms ($p > 0.05$) are presented. **(C)** Volcano plot analysis of proteins detected in IACs isolated from RPMI-7951 cells transiently transfected with non-specific siRNA (si(-)) versus integrin αV-specific siRNA (si(αV)). IAC proteins are visualized as volcano plot after the analysis with QSpec/QProt to generate -Log (FDR) and fold change values. Cut off values of −Log (FDR) ≥ 1 (red horizontal dotted line) corresponding to FDR ≤ 0.05 and −Log (FDR) ≥ 1,3 (black horizontal dotted line) corresponding to FDR ≤ 0.1; and fold change ≥ 1.5 (black vertical dotted line) or 2 (red vertical dotted line) were used. Each dot on the plot represents one protein. Proteins with significantly different abundance between IACs of si(αV) and si(-) cells and of interest for this paper were marked with their gene name. Upper left quadrant – proteins detected with lower levels of spectra in si(αV), upper right quadrant – proteins detected with higher levels of spectra in si(αV). For this analysis, only proteins identified with a minimal number of spectral counts ≥ 4 in at least one biological replicate, FDR < 5%, probability for protein identification ≥ 99.9% were visualized. **(D)** Proteins from (C) with FDR≤ 0.1 and fold change ≥ (green) or ≤ (red) 1.5 were separately assigned to functional groups using DAVID GO database (GOTERM_CC_DIRECT). Statistically significant GO terms were presented in reverse x-axis of p-value (the smaller the p-value - the bigger the length of the bar). Green represents GO terms annotated to the proteins whose abundance is higher in si(αV) then si(-) and green to reverse. The p-value represents Benjamini corrected p-value. ↓, decreased abundance, ↑, increased abundance.

Fig. 2 Talin2 and KANK2 differentially affect cell sensitivity to PTX and cell migration. In RPMI-7951 cells **(A)** talin2 knockdown increases sensitivity to PTX, while **(B)** KANK2 knockdown decreases it. Twenty-four hours upon transfection, cells were seeded in 96-well plates and 24 hours later treated with different concentrations of PTX. Cytotoxicity was measured by MTT assay. Data were analysed by two-way analysis of variance (ANOVA) with Šídák's multiple comparisons test, with a single pooled variance. ns, not significant; *P < 0.05; **P < 0.01; ***P < 0.001; ****P < 0.0001. (n = 3). **(C)** Talin2 knockdown decreases, and KANK2 knockdown increases migration in RPMI-7951 cells. Serum starved (24 hours) cells, transfected previously with either control or talin2-specific siRNA were seeded in Transwell cell culture inserts and left to migrate for 22 hours toward serum. Cells on the underside of the inserts were stained with crystal violet, photographed, and counted. Scale bar = 100 μm. Histogram data represents averages of five microscope fields of three independently performed experiments, plotted as mean ± SD. Data were analysed by unpaired Student's t-test. ns, not significant; *P < 0.05; **P < 0.01; ***P < 0.001; ****P < 0.0001.

Fig. 3 Talin1 is necessary for maintenance of integrin αVβ5 FAs, while talin2 influences their dynamics. (A) Talin1 and talin2 are localized within integrin αVβ5 FAs. Forty-eight hours after seeding, RPMI-7951 cells were methanol fixed, and stained with anti-talin1 antibody followed by Alexa-Fluor IgG1 555-conjugated antibody (red), anti-talin2 antibody followed by Alexa-Fluor IgG2b 488-conjugated antibody (green) and anti-integrin β5 antibody followed by Alexa-Fluor 647-conjugated antibody (magenta) and IRM images were taken. Analysis was performed using TCS SP8 Leica. Scale bar = 10 μm. **(B)** Integrin β5 and talin2 are in close proximity. Forty-eight hours after seeding RPMI-7951 cells were methanol fixed, and a PLA assay with anti-integrin β5 and anti-talin2 primary antibody was performed. Generated fluorescent dots were visualized and IRM images were taken. Analysis was performed using TCS SP8 Leica. Scale bar = 10 μm. **(C)** Talin1 knockdown, disrupts αVβ5 FAs and a reduces cell size, while talin2 knockdown only increased size of talin1-positive structures and reduced the number of integrin β5-positive structures. Forty-eight hours after transfection with either control siRNA, talin1 or talin2-specific siRNA, RPMI-7951 cells were methanol fixed, and stained with anti-talin1 antibody followed by Alexa-Fluor IgG1 555-conjugated antibody (red), anti-talin2 antibody followed by Alexa-Fluor IgG2b 488-conjugated antibody (green) and anti-β5 antibody followed by Alexa-Fluor 647-conjugated antibody (magenta) and IRM images were taken. Analysis was performed using TCS SP8 Leica. Scale bar = 10 μm. **(D, E)** Quantification of data presented in (C) Violin plots (number of structures/cell) and scatter plots with median marked in size (cell size, size of structures/cell) represents measurements of > 45 cells. Data were analysed by one-way ANOVA with Dunnett's multiple comparison. ns, not significant; * P < 0.05; ** P < 0.01; *** P < 0.001; **** P < 0.0001.

Fig. 4 In RPMI-7951 cells talin1 localizes with KANK2 predominantly at the cell edge while talin2 and KANK2 localize predominantly in the cell centre. (A) KANK2 localizes in talin1 and talin2-positive adhesions. Forty-eight hours after seeding RPMI-7951 cells were methanol fixed, and stained with anti-talin1 antibody followed by Alexa-Fluor IgG1 555-conjugated antibody (red), anti-talin2 antibody followed by Alexa-Fluor IgG2b 488-conjugated antibody (green) and anti-KANK2 antibody followed by Alexa-Fluor 647-conjugated antibody (magenta) and IRM images were taken. Analysis was performed using TCS SP8 Leica. Scale bar = 10 μm. **(B)** KANK2 is in close proximity with talin1 and talin2. Forty-eight hours after seeding cells were methanol fixed, and a PLA assay using anti-KANK2 combined with either anti-talin1 or anti-talin2 primary antibody was performed. Generated fluorescent dots were visualized and IRM images were taken. Analysis was performed using TCS SP8 Leica. Scale bar = 10 μm. **(C)** Quantification of data presented in (B). Violin plots (percentage of positive signal/cell) represents measurements of > 30 cells. Data were analysed by one-way ANOVA with Dunnett's multiple comparison. ns, not significant; * $P < 0.05$; ** $P < 0.01$; *** $P < 0.001$; **** $P < 0.0001$. **(D)** Knockdown of talin1, unlike talin2, leads to changes in KANK2 localization. Forty-eight hours after transfection with either control siRNA, talin1 or talin2-specific siRNA, RPMI-7951 cells were methanol fixed and stained with anti-talin1 antibody followed by Alexa-Fluor IgG1 555-conjugated antibody (red), anti-talin2 antibody followed by Alexa-Fluor IgG2b 488-conjugated antibody (green), anti-KANK2 antibody followed by Alexa-Fluor 647-conjugated antibody (magenta) and IRM images were taken. Analysis was performed using TCS SP8 Leica. Scale bar = 10 μm. **(E)** Quantification of data presented in (D). Violin plot (number of structures/cell) and scatter plot with median marked in size (cell size, size of structures/cell) represents measurements of > 45 cells. Data were analysed by one-way ANOVA with Dunnett's multiple comparison. ns, not significant; * $P < 0.05$; ** $P < 0.01$; *** $P < 0.001$; **** $P < 0.0001$.

Fig. 5 In RPMI-7951 cells KANK2 is part of FAs, FBs, RAs. (A) KANK2 localizes in integrin α5-positive structures. Forty-eight hours after seeding RPMI-7951 cells were fixed and permeabilised, and stained with anti-integrin α5 antibody followed by Alexa-Fluor 546-conjugated antibody (red), anti-KANK2 antibody followed by Alexa-Fluor 488-conjugated antibody (green) and IRM images were taken. Analysis was performed using TCS SP8 Leica. Scale bar = 10 μm. **(B)** KANK2 is in close proximity with integrin α5. Forty-eight hours after seeding cells were PFA fixed and permeabilised, and a PLA assay using anti-KANK2 combined with anti-integrin α5 primary antibody was performed. Generated fluorescent dots were visualized and IRM images were taken. Analysis was performed using TCS SP8 Leica. Scale bar = 10 μm. **(C)** Effect of knockdown of integrin α5 or KANK2 on cell size, the number and size of talin1 and talin2 structures. Forty-eight hours after transfection with either control siRNA, integrin α5 or KANK2-specific siRNA, RPMI-7951 cells were methanol fixed and stained with anti-talin1 antibody followed by Alexa-Fluor IgG1 555-conjugated antibody (red), anti-talin2 antibody followed by Alexa-Fluor IgG2b 488-conjugated antibody (green), anti-KANK2 antibody followed by Alexa-Fluor 647-conjugated antibody (magenta) and IRM images were taken. Analysis was performed using TCS SP8 Leica. Scale bar = 10 μm. **(D, E)** Quantification of data presented in (C). Violin plots (number of structures/cell) and scatter plots with median marked in size (cell size, size of structures/cell) represents measurements of > 45 cells. Data were analysed by one-way ANOVA with Dunnett's multiple comparison. ns, not significant; * $P < 0.05$; ** $P < 0.01$; *** $P < 0.001$; **** $P < 0.0001$.

Fig. 6 In RPMI-7951 cells KANK2 is in close proximity to talin2 in FAs, FBs, RAs. (A, C) KANK2 knockdown increases integrin α5-positive structures, but has no effect on integrin β5-positive structures. Forty-eight hours after transfection with either control siRNA or KANK2-specific siRNA RPMI-7951 cells were fixed and permeabilised, and stained with (A) anti-integrin α5 antibody followed by Alexa-Fluor 546-conjugated antibody (red) and anti-KANK2 antibody followed by Alexa-Fluor 488-conjugated antibody (green) or (B) anti-talin2 antibody followed by Alexa-Fluor IgG2b 488-conjugated antibody (green) and anti-KANK2 antibody followed by Alexa-Fluor 647-conjugated antibody (magenta). IRM images were taken. Analysis was performed using TCS SP8 Leica. Scale bar = 10 μm. **(B, D)** Quantification of data presented in (A, C respectively). Violin plots (number of structures/cell) and scatter plots with median marked in size (cell size, size of structures/cell) represents measurements of > 45 cells. Data were analysed by one-way ANOVA with Dunnett's multiple comparison. ns, not significant; * $P < 0.05$; ** $P < 0.01$; *** $P < 0.001$; **** $P < 0.0001$. **(E)** Knockdown of integrin α5 or integrin β5 influences the distribution of talin2 KANK2 proximity signal in RPMI-7951 cells. Forty-eight hours after transfection with either control siRNA, integrin α5- or integrin β5-specific siRNA RPMI-7951 cells were methanol fixed and a PLA assay using anti-KANK2 combined with anti-talin2 primary antibody was performed. Generated fluorescent dots were visualized and IRM images were taken. Analysis was performed using TCS SP8 Leica. Scale bar = 10 μm. (F) Quantification of

data presented in (E). Violin plots (percentage of positive signal/cell) represents measurements of > 20 cells. Data were analysed by one-way ANOVA with Dunnett's multiple comparison. ns, not significant; * P < 0.05; ** P < 0.01; *** P < 0.001; **** P < 0.0001.

Fig. 7 Loss of integrin α5 or KANK2 from FBs increases cell migration through changes in MT cytoskeleton. **(A)** Integrin α5 or KANK2 knockdown decreases migration in RPMI-7951 cells. Serum starved (24 hours) cells, transfected previously with either control, integrin α5- or KANK2-specific siRNA were seeded in Transwell cell culture inserts and left to migrate for 22 hours toward serum. Cells on the underside of the inserts were stained with crystal violet, photographed, and counted. Scale bar = 100 μm. **(B)** Histogram data represents averages of five microscope fields of three independently performed experiments, plotted as mean ± SD. Data were analysed by unpaired Student's t-test. ns, not significant; *P < 0.05; **P < 0.01; ***P < 0.001; ****P < 0.0001. **(C)** Talin1 knockdown disrupts actin and MT cytoskeleton, while talin2 knockdown alters MT cytoskeleton in a manner distinct from that of integrin α5 or KANK2 knockdown. Visualization of α-tubulin and F-actin upon knockdown of talin1, talin2, integrin α5 and KANK2. Forty-eight hours after transfection with either control, talin1-specific (si(talin1), talin2-specific (si(talin2)), integrin α5-specific (si(ITGA5)) or KANK2-specific (si(KANK2)) siRNA. RPMI-7951 cells were fixed with methanol (for α-tubulin visualization) or PFA followed by permeabilization with Triton X-100 (for F-actin visualization), and stained with anti-α-tubulin antibody followed by Alexa-Flour 647-conjugated antibody (magenta) and IRM images were taken. For F-actin visualization cells were incubated with Alexa-Flour 488 conjugated phalloidin (shown in gold). Analysis was performed using TCS SP8 Leica. Scale bar = 10 μm. **(D, E)** Quantification of data presented in (C). Violin plots represents measurements of > 40 cells. Data were analysed by unpaired Student's t-test. ns, not significant; *P < 0.05; **P < 0.01; ***P < 0.001; ****P < 0.0001.

Fig. 1

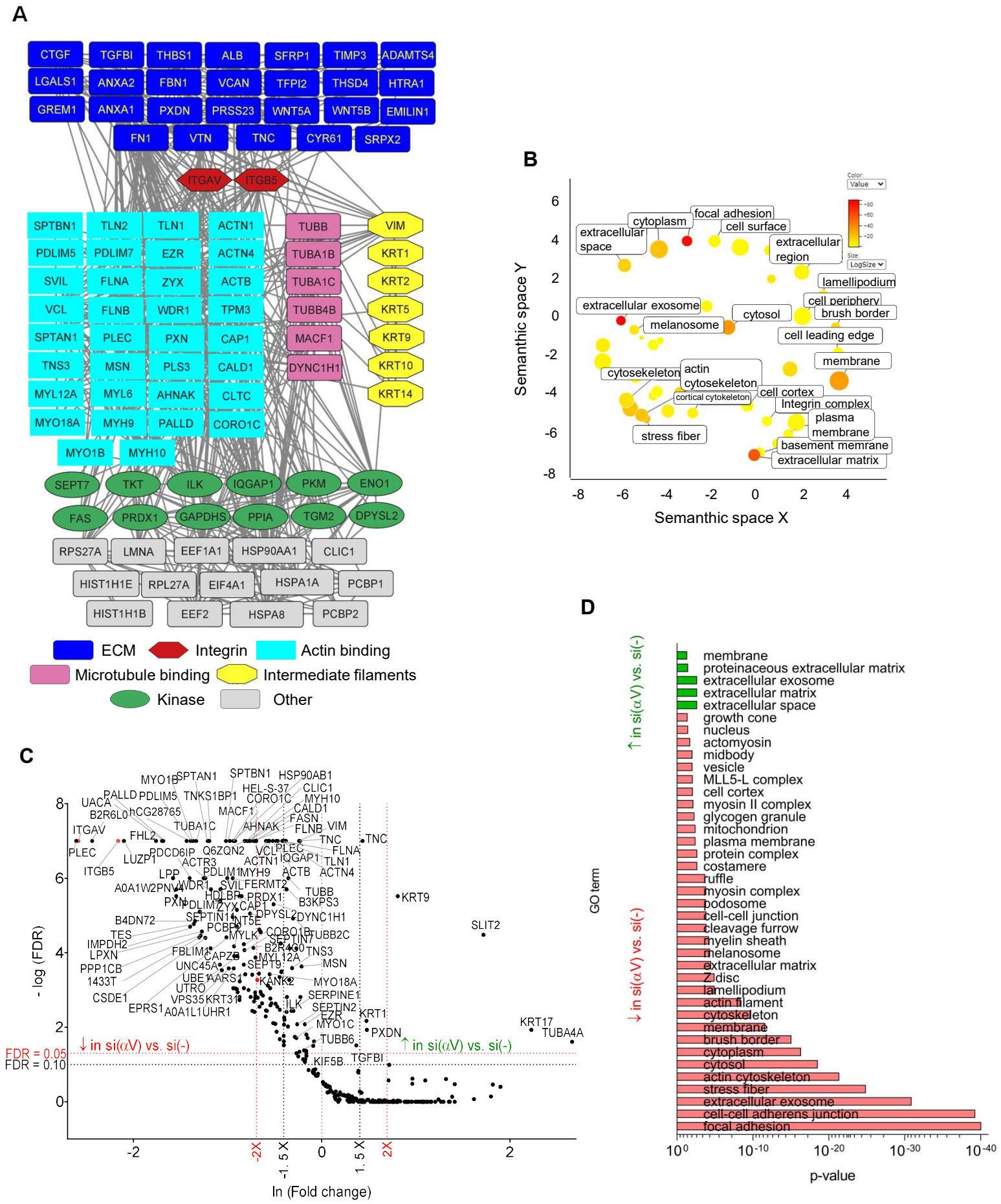
A
CTGF
TGFBI
THBS1
ALB
SFRP1
TIMP3
ADAMTS4
LGALS1
ANXA2
FBN1
VCAN
TFPI2
THSD4
HTRA1
GREM1
ANXA1
PXDN
PRSS23
WNT5A
WNT5B
EMILIN1
FN1
VTN
TNC
CYR61
SRPX2
ITGAV
ITGB5
SPTBN1
TLN2
TLN1
ACTN1
PDLIM5
PDLIM7
EZR
ACTN4
SVIL
FLNA
ZYX
ACTB
VCL
FLNB
WDR1
TPM3
SPTAN1
PLEC
PXN
CAP1
TNS3
MSN
PLS3
CALD1
MYL12A
MYL6
AHNAK
CLTC
MYO18A
MYH9
PALLD
CORO1C
MYO1B
MYH10
TUBB
TUBA1B
TUBA1C
TUBB4B
MACF1
DYNC1H1
VIM
KRT1
KRT2
KRT5
KRT9
KRT10
KRT14
SEPT7
TKT
ILK
IQGAP1
PKM
ENO1
FAS
PRDX1
GAPDHS
PPIA
TGM2
DPYSL2
RPS27A
LMNA
EEF1A1
HSP90AA1
CLIC1
HIST1H1E
RPL27A
EIF4A1
HSPA1A
PCBP1
HIST1H1B
EEF2
HSPA8
PCBP2
ECM
Integrin
Actin binding
Microtubule binding
Intermediate filaments
Kinase
Other
B
Semanthic space Y
Semanthic space X
extracellular space
cytoplasm
focal adhesion
cell surface
extracellular region
lamellipodium
extracellular exosome
cell periphery
brush border
melanosome
cytosol
cell leading edge
membrane
cytosekeleton
actin cytosekeleton
cortical cytokeleton
cell cortex
Integrin complex
plasma membrane
stress fiber
basement memrane
extracellular matrix
C
- log (FDR)
ln (Fold change)
FDR = 0.05
FDR = 0.10
↓ in si(αV) vs. si(-)
↑ in si(αV) vs. si(-)
-2X
-1. 5 X
1. 5 X
2X
KRT9
SLIT2
KRT17
TUBA4A
KRT1
PXDN
TGFBI
D
GO term
p-value
membrane
proteinaceous extracellular matrix
extracellular exosome
extracellular matrix
extracellular space
growth cone
nucleus
actomyosin
midbody
vesicle
MLL5-L complex
cell cortex
myosin II complex
glycogen granule
mitochondrion
plasma membrane
protein complex
costamere
ruffle
myosin complex
podosome
cell-cell junction
cleavage furrow
myelin sheath
melanosome
extracellular matrix
Z disc
lamellipodium
actin filament
cytoskeleton
membrane
brush border
cytoplasm
cytosol
actin cytoskeleton
stress fiber
extracellular exosome
cell-cell adherens junction
focal adhesion

Fig. 2

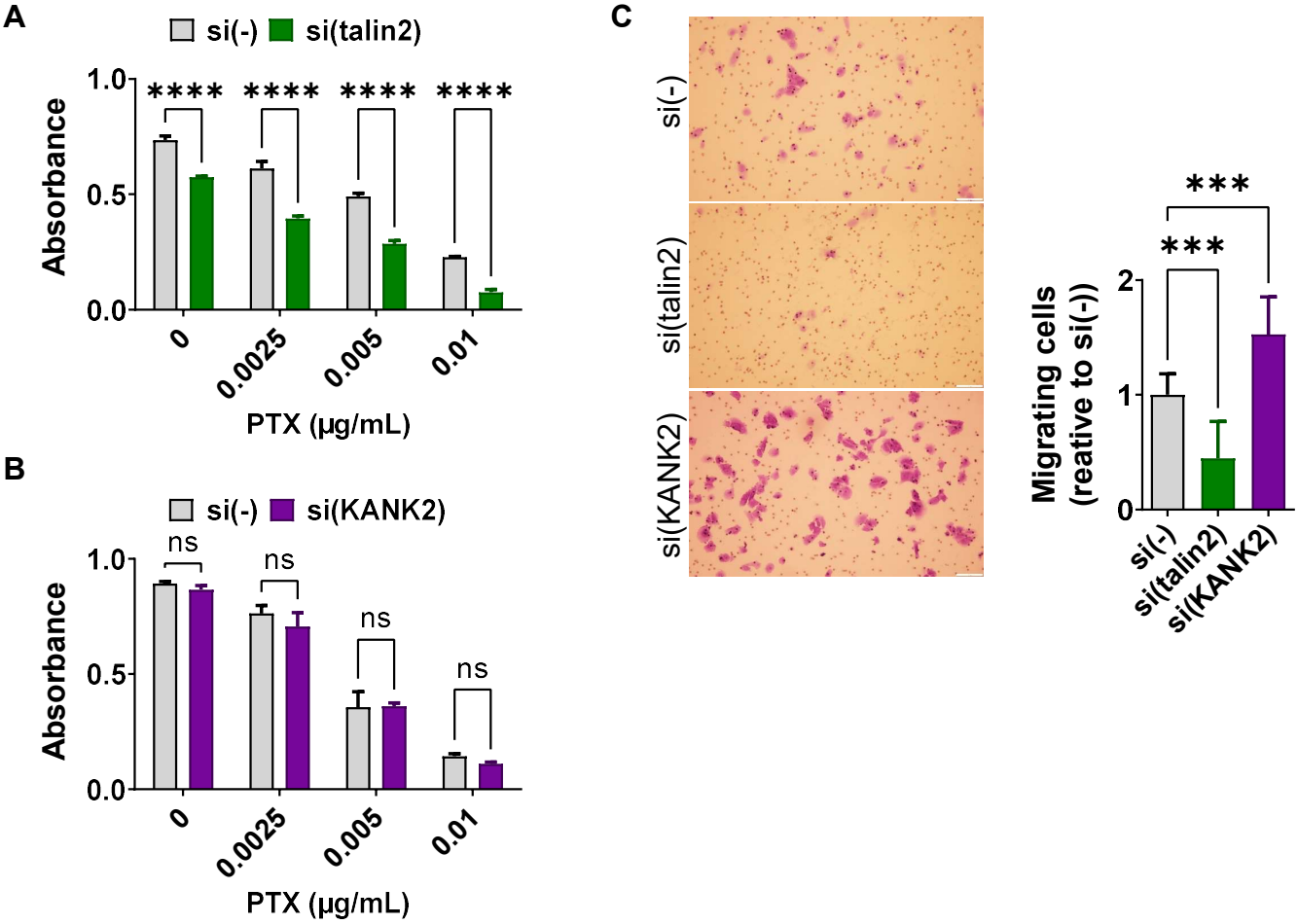
A
si(-)
si(talin2)
Absorbance
1.0
0.5
0.0
****
****
****
****
0
0.0025
0.005
0.01
PTX (μg/mL)
B
si(-)
si(KANK2)
Absorbance
1.0
0.5
0.0
ns
ns
ns
ns
0
0.0025
0.005
0.01
PTX (μg/mL)
C
si(-)
si(talin2)
si(KANK2)
Migrating cells
(reative to si(-))
2
1
0
***
***
si(-)
si(talin2)
si(KANK2)

Fig. 3

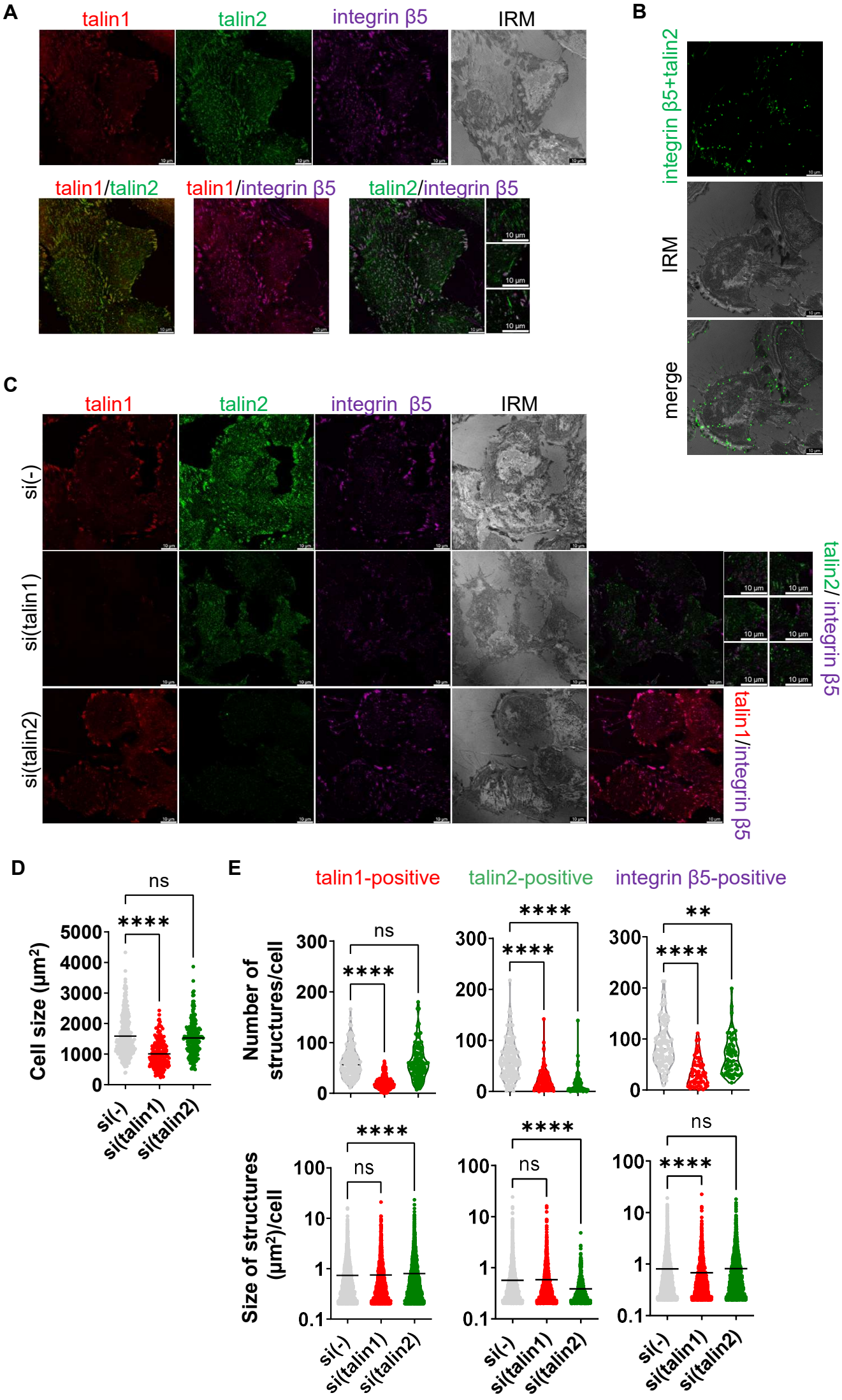
A
talin1
talin2
integrin β5
IRM
talin1/talin2
talin1/integrin β5
talin2/integrin β5
B
integrin β5+talin2
IRM
merge
C
talin1
talin2
integrin β5
IRM
si(-)
si(talin1)
si(talin2)
talin2/ integrin β5
talin1/integrin β5
D
Cell size (μm²)
ns
****
si(-)
si(talin1)
si(talin2)
E
talin1-positive
talin2-positive
integrin β5-positive
Number of structures/cell
Size of structures (μm²)/cell
ns
****
**

Fig. 4

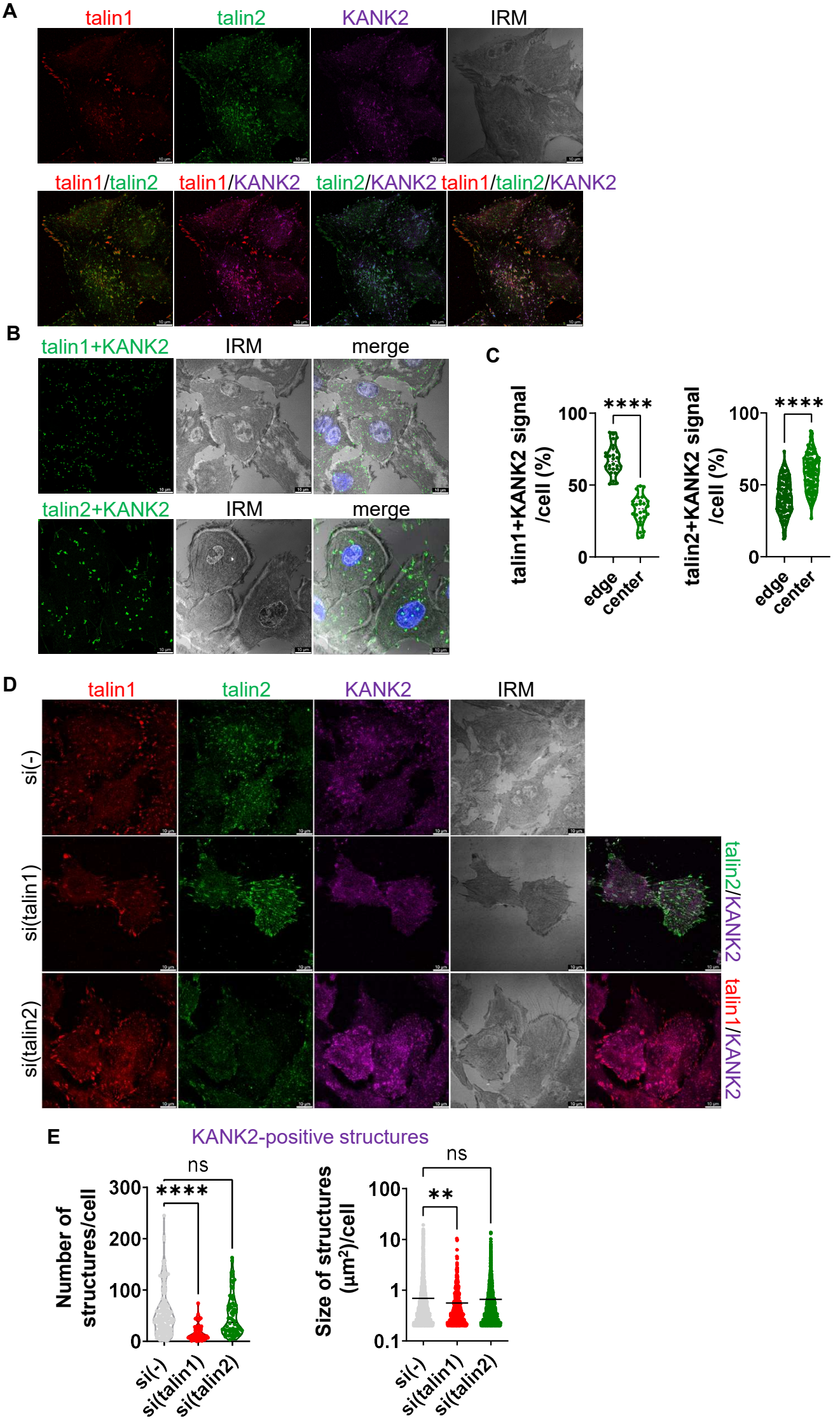
A
talin1
talin2
KANK2
IRM
talin1/talin2
talin1/KANK2
talin2/KANK2
talin1/talin2/KANK2
B
talin1+KANK2
IRM
merge
talin2+KANK2
IRM
merge
C
talin1+KANK2 signal /cell (%)
****
100
50
0
edge
center
talin2+KANK2 signal /cell (%)
****
100
50
0
edge
center
D
talin1
talin2
KANK2
IRM
si(-)
si(talin1)
si(talin2)
talin2/KANK2
talin1/KANK2
E
KANK2-positive structures
Number of structures/cell
ns
****
300
200
100
0
si(-)
si(talin1)
si(talin2)
Size of structures (μm²)/cell
ns
**
100
10
1
0.1
si(-)
si(talin1)
si(talin2)

Fig. 5

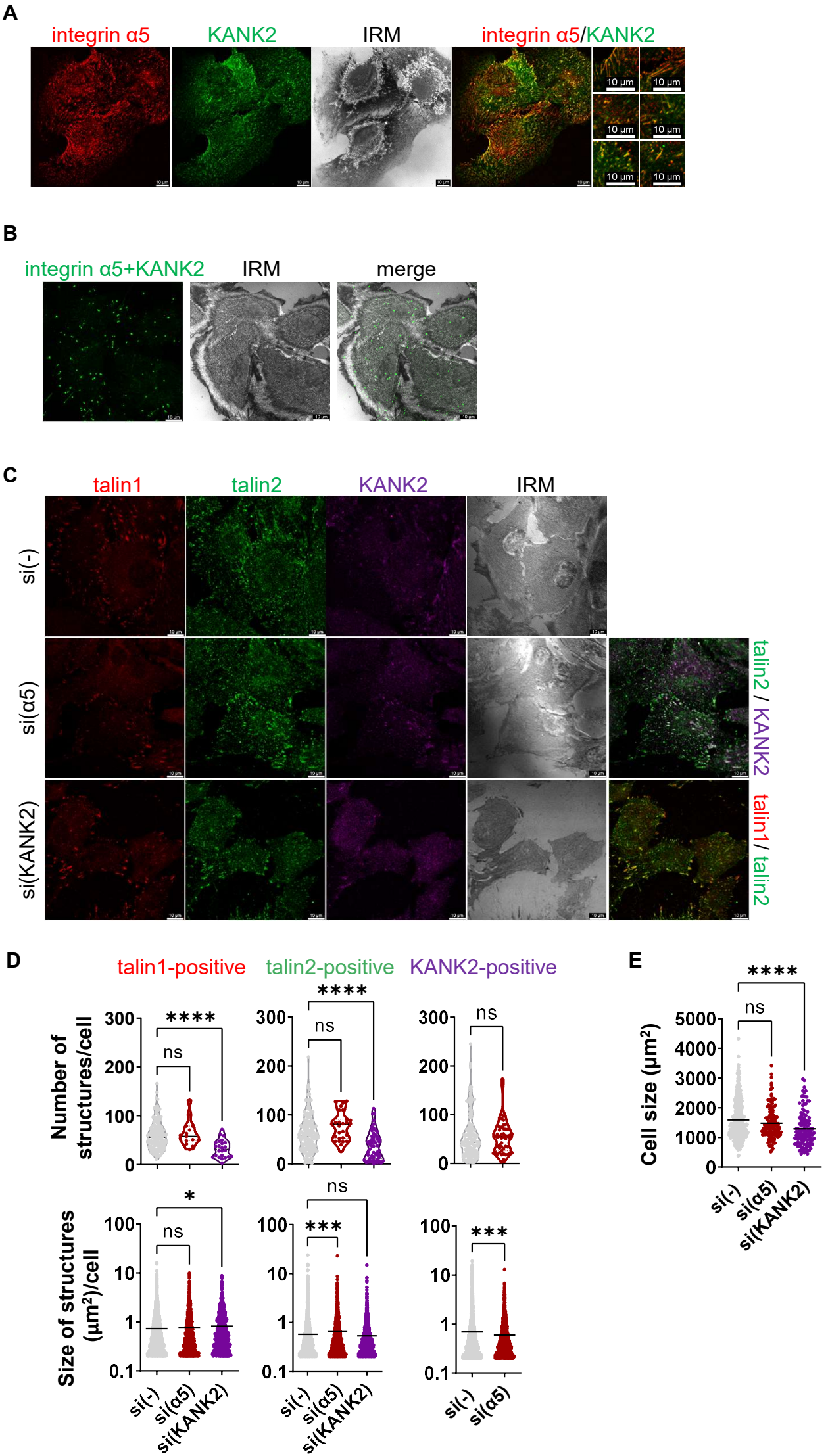
A
integrin α5
KANK2
IRM
integrin α5/KANK2
10 μm
B
integrin α5+KANK2
IRM
merge
C
talin1
talin2
KANK2
IRM
si(-)
si(α5)
si(KANK2)
talin2 / KANK2
talin1 / talin2
D
talin1-positive
talin2-positive
KANK2-positive
Number of structures/cell
Size of structures (μm²)/cell
****
ns
*
***
si(-)
si(α5)
si(KANK2)
E
Cell size (μm²)
si(-)
si(α5)
si(KANK2)

Fig. 6

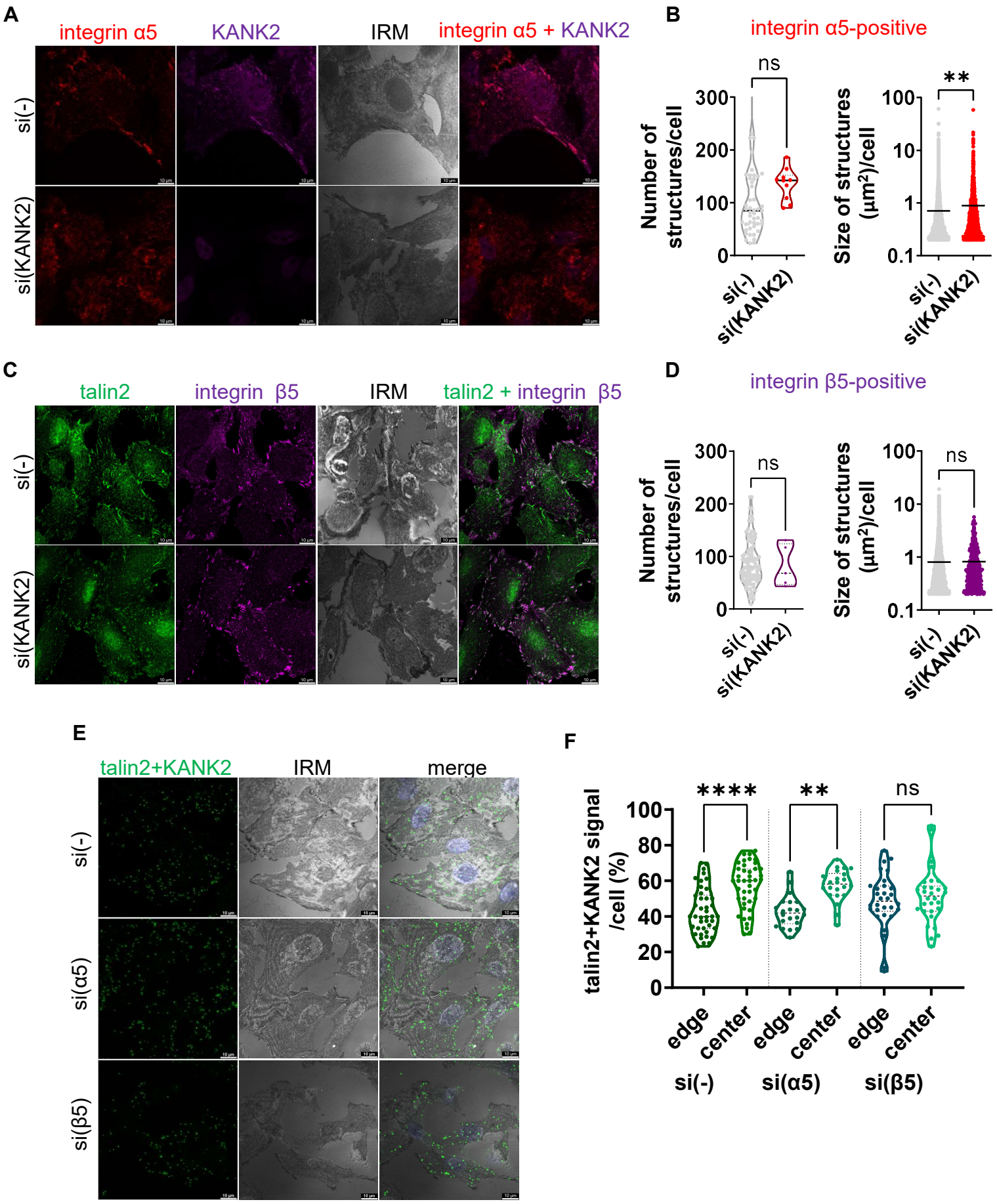
A
integrin α5
KANK2
IRM
integrin α5 + KANK2
si(-)
si(KANK2)
B
integrin α5-positive
ns
**
Number of structures/cell
Size of structures (μm²)/cell
300
200
100
0
100
10
1
0.1
si(-)
si(KANK2)
C
talin2
integrin β5
IRM
talin2 + integrin β5
si(-)
si(KANK2)
D
integrin β5-positive
ns
ns
Number of structures/cell
Size of structures (μm²)/cell
si(-)
si(KANK2)
E
talin2+KANK2
IRM
merge
si(-)
si(α5)
si(β5)
F
talin2+KANK2 signal /cell (%)
****
**
ns
100
80
60
40
20
0
edge
center
edge
center
edge
center
si(-)
si(α5)
si(β5)

Fig. 7

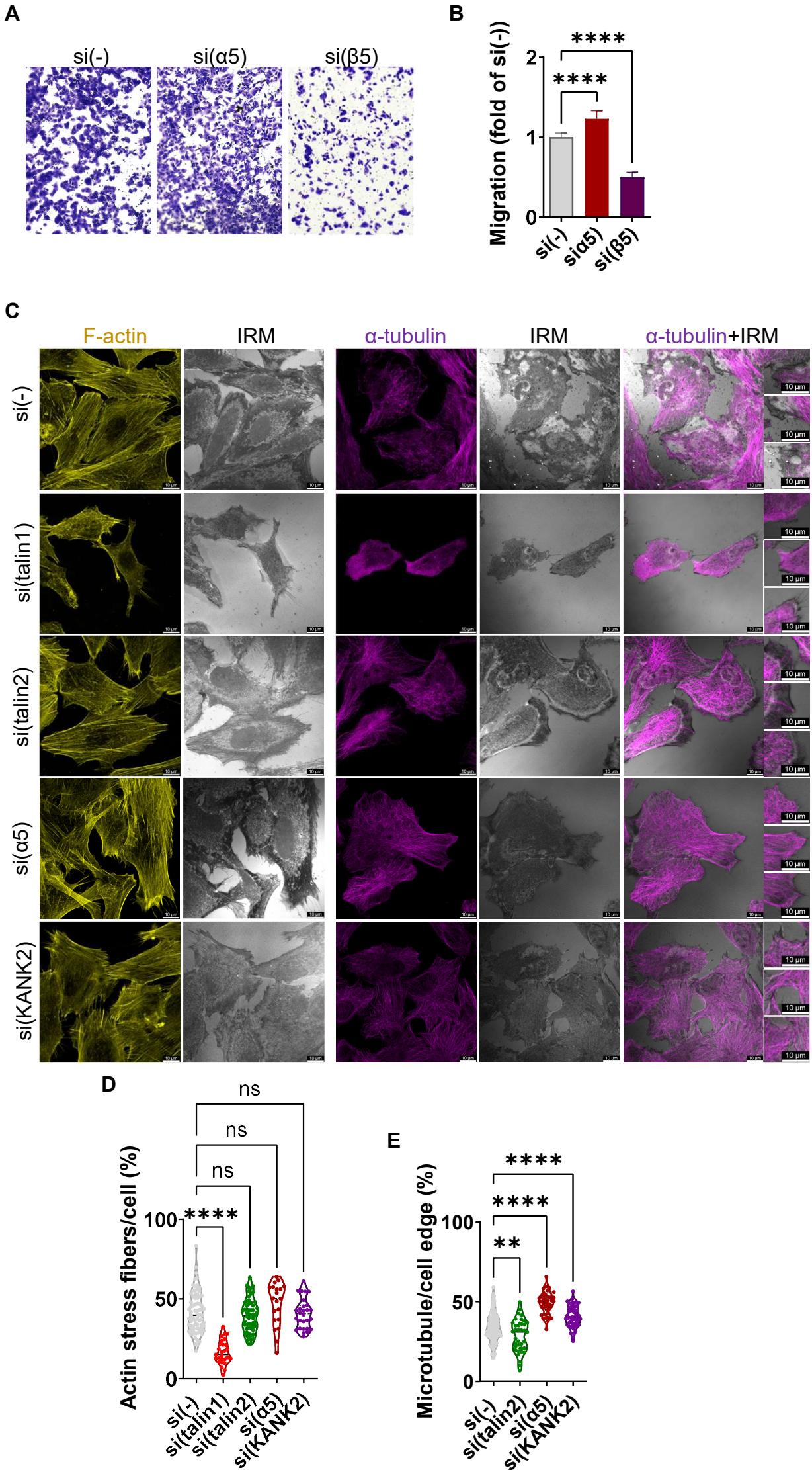
A
si(-)
si(α5)
si(β5)
B
Migration (fold of si(-))
****
****
2
1
0
si(-)
siα5)
si(β5)
C
F-actin
IRM
α-tubulin
IRM
α-tubulin+IRM
si(-)
si(talin1)
si(talin2)
si(α5)
si(KANK2)
10 μm
D
Actin stress fibers/cell (%)
ns
ns
ns
****
100
50
0
si(-)
si(talin1)
si(talin2)
si(α5)
si(KANK2)
E
Microtubule/cell edge (%)
****
****
**
100
50
0
si(-)
si(talin2)
si(α5)
si(KANK2)